Atmospheric Research 304 (2024) 107341

Contents lists available at ScienceDirect

Atmospheric Research

journal homepage: www.elsevier.com/locate/atmosres

Formation mechanisms of persistent extreme precipitation events over the eastern periphery of the Tibetan Plateau: Synoptic conditions, moisture transport and the effect of steep terrain

Ruiyu Zhao [a,b], Bin Chen [b,*], Wei Zhang [c], Shuai Yang [d], Xiangde Xu [b]

[a] Department of Atmospheric and Oceanic Sciences, Institute of Atmospheric Sciences, Fudan University, 200438 Shanghai, China
[b] State Key Laboratory of Severe Weather, Chinese Academy of Meteorological Sciences, Beijing 100081, China
[c] Utah State University: Logan, Utah, United States of America
[d] Laboratory of Cloud-Precipitation Physics and Severe Storms (LACS), Institute of Atmospheric Physics, Chinese Academy of Sciences, Beijing 100029, China

ARTICLE INFO

Keywords:
Persistent extreme precipitation
Tibetan Plateau
Moisture source
Atmospheric circulation anomalies
Steep terrain

ABSTRACT

The eastern periphery of the Tibetan Plateau (EPTP) is prone to frequent and severe Persistent Extreme precipitation (PEP) events in summer. Given the complexity of weather systems and the intricate nature of terrain over this region, the generation and development mechanisms of the PEP in the EPTP remain to be determined. In this study, the formation and persistence mechanisms are further explored from the perspective of the general features of large-scale circulations, moisture source diagnosis and the influence of steep topography by using a thermal-dynamical diagnosis method, a mesoscale numerical simulation and a Lagrangian identification of the main moisture sources. The results show that during PEP events, the corresponding atmospheric circulation systems are characterized by an anomalous Rossby wave train at middle levels, an intensified westerly jet, an eastward extension of the South Asian high and a westward extension of the western Pacific subtropical high, all of which are possible to facilitate the development of potential instability and anticyclonic convergence of water vapor transport. The evaporative moisture sources from the Southeastern Asia (SEA), Bay of Bengal (BOB), and Southern China Sea (SCS) are remarkably enhanced during PEP events, with a contribution of 56.44%, which is 28.5% higher than the climatic mean. The further sensitive experiment indicates that the steep terrain could enhance the continuous transport of positive potential vorticity and the downward propagation of upper-level isentropic potential vorticity disturbances, thereby playing an essential role in the triggering and development of PEP events.

1. Introduction

The eastern periphery of the Tibetan Plateau (EPTP), located at the area of 29.8°N–31.5°N, 102.6°E–104.5°E (Fig. 1a), acts as a transition zone of the Indian monsoon and the East Asian monsoon, and it is bordered by the Tibetan Plateau (TP) to the west and the Sichuan Basin to the east. This region is characterized by highly complex topography and steep slopes ranging from about half of the troposphere height to the plain within a few hundred kilometers (Hu and Yuan, 2021). Due to the combined effects of various synoptic systems, complex terrain and unique location (Wang and Ho, 2002), the EPTP region is one of the predominant summer rainfall regions in the world (Chen et al., 2016; Luo et al., 2020). The well-known "Rainy City", Ya'an, which has the maximum annual precipitation and rainy days in the mainland of China, is located in the EPTP region (Li et al., 2010; Chen et al., 2018a). In addition, global warming has further exacerbated the frequency and intensity of extreme precipitation following the Clausius-Clapeyron relation in recent years (Trenberth, 1998; Dai and Nie, 2022). Extreme precipitation events on the TP show an increasing trend as well (You et al., 2008; Ding et al., 2021), resulting in larger ramifications that threaten the safety of millions of lives and economic development. Considering that the Sichuan Basin and its adjacent areas are one of the most densely populated regions in China, understanding the formation mechanisms of summer rainfall in the EPTP region is of great significance to local communities and deserves more attention.

Due to the complex geography and climatic conditions, the causes of extreme precipitation in this region are rather intricate. In recent years, many efforts have been made to reveal the underlying mechanisms of

* Corresponding author.
E-mail address: chenbin@cma.gov.cn (B. Chen).

https://doi.org/10.1016/j.atmosres.2024.107341
Received 19 January 2024; Received in revised form 28 February 2024; Accepted 10 March 2024
Available online 12 March 2024

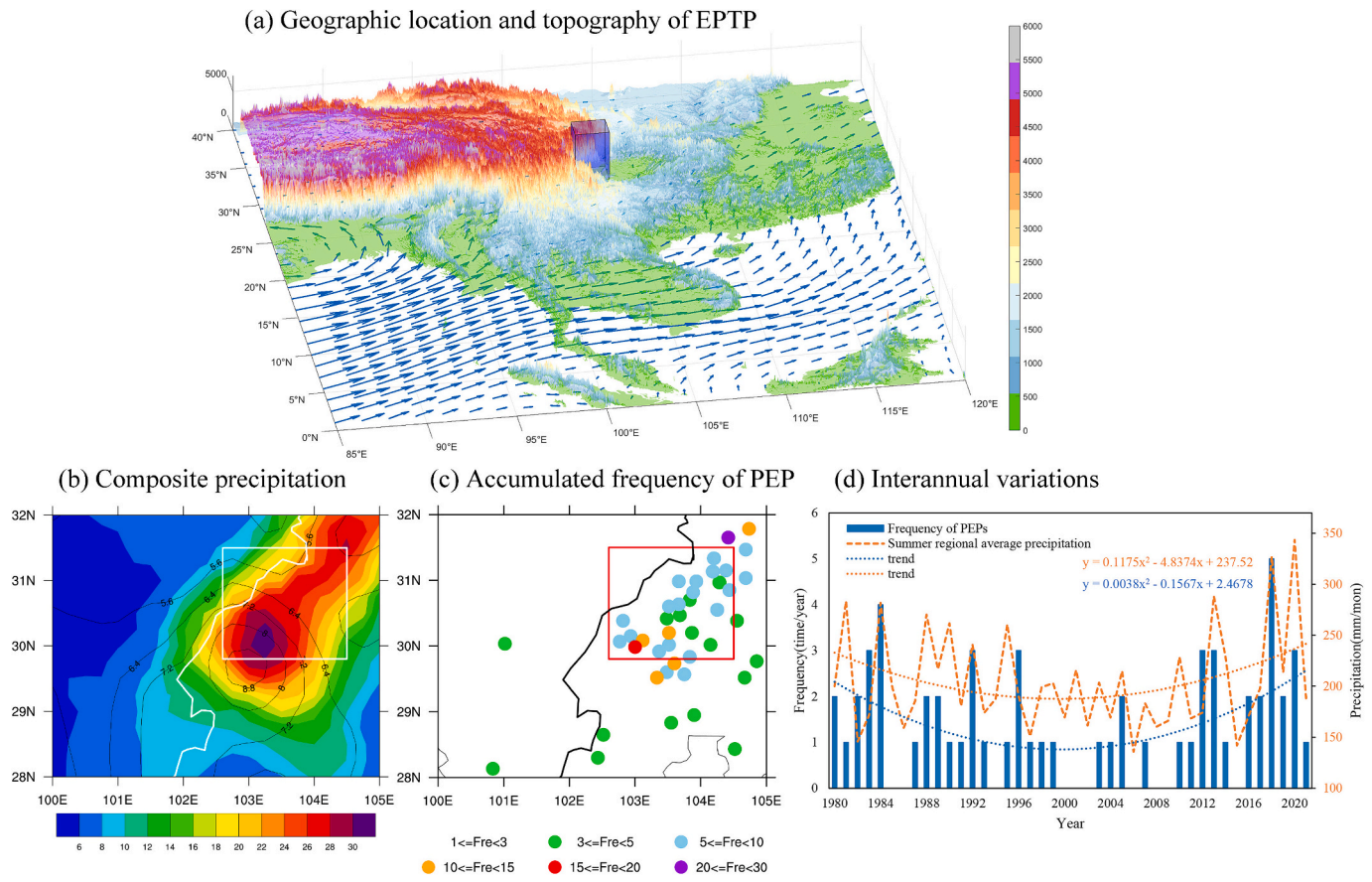

Fig. 1. (a) The geographical location (blue column) and topography (color shaded areas, m) of the eastern periphery of the Tibetan Plateau (EPTP), (b) the distributions of the composite average rainfall amounts (mm d^{-1}) during the summer (June, July and August) of 1980–2021 (contours) and 60 persistent Extreme precipitation (PEP) events (shaded areas) over the EPTP, (c) the distribution of the accumulated frequency of persistent Extreme precipitation at various stations during the summer (June, July and August) of 1980–2021, and (d) interannual variations of persistent Extreme precipitation frequency (bars) and regional mean precipitation (dash lines) over the EPTP. The vector in Fig. 1a represents the integrated average water vapor flux in summer, and the white and red rectangular in Fig. 1b and Fig. 1c indicates the EPTP. (For interpretation of the references to color in this figure legend, the reader is referred to the web version of this article.)

extreme precipitation events over the EPTP and its adjacent regions. Previous studies have shown that heavy rainfall in the EPTP is a consequence of the interactions of multiscale physical processes (Liu et al., 2018), such as active small-scale convection activities (Fu et al., 2019), mesoscale systems including southwest vortexes or plateau vortexes (Fu et al., 2015; Fu et al., 2019; Zhou et al., 2019; Meng et al., 2021; Chen et al., 2022; Mai et al., 2021), adjustments in the configuration of large-scale circulation systems (Hu et al., 2021; Nie and Sun, 2021; Xu et al., 2023), water vapor transport processes (Huang and Cui, 2015; Chen et al., 2016; Yang et al., 2010), the forces of complex topography (Lu., 2019; Hu et al., 2021) and even the activities of remote tropical cyclones (Zhang et al., 2017a; Yi et al., 2020; Yuan et al., 2018).

In terms of the adjustments in atmospheric circulation configuration, the location and intensity of sub-members of the Asian summer monsoon system, such as the South Asian high (SAH), the western Pacific subtropical high (WPSH), the Indian-Myanmar trough and the East Asian colder trough, have been suggested to be the drivers that are closely associated with the occurrence of extreme rainfall (Chen et al., 2016; Zhou and Wang, 2019; Hu et al., 2021; Xia et al., 2021; Nie and Sun, 2021; Zhang et al., 2017b; Chen et al., 2022; Qian et al., 2022; Xu et al., 2023). Specifically, Zhang et al. (2017b) pointed out that the westward extension of the WPSH could drive tropical cyclones southward, thereby contributing to the occurrence of extreme precipitation in eastern China. Nie and Sun (2021) noted that an atmospheric wave train propagates approximately one week before heavy rainfall over Southwest China, which may result in an anomalous low-pressure system over the eastern TP. Recently, Xu et al. (2023) showed that the large-scale circulations responsible for the summer heavy rainfall events over the Sichuan Basin are characterized by the configuration of an eastward-extending SAH, a westward-extending WPSH and an apparent low-level vortex. Several studies also highlighted TP vortexes and southwest vortexes (Fu et al., 2020; Fu et al., 2019; Ni et al., 2017; Li et al., 2020; Mai et al., 2021). In addition, Wu and Luo (2019) pointed out that low-level shear lines are the main synoptic pattern over the Sichuan Basin, and Liu et al. (2018) also emphasized the interaction between low-level shear lines and the large-scale circulation pattern. In general, the existing studies mostly focus on a specific event, and lack a systematic exploration on the circulation configuration for the persistent precipitation events.

In addition to complex weather systems, water vapor transport is also an essential prerequisite for the formation of Extreme precipitation. In terms of the precipitation on the southeastern TP, the water vapor transport is affected by both the Indian summer monsoon and the East Asian monsoon (Xu et al., 2014; Dong et al., 2016; Chen et al., 2019), displaying remarkable multi-scale spatio-temporal variabilities (Chen et al., 2016, 2019). Numerous studies have been carried out based on the Eulerian or Lagrangian approach to determine the moisture sources around the EPTP and its adjacent regions and their association with precipitation. Within the Eulerian framework, for example, Feng and Zhou (2012) demonstrated that the water vapor originating from the Indian Ocean and the Bay of Bengal supplies the summer moisture on the southeastern TP. This was further confirmed by Pan et al. (2018) based on the Community Atmosphere Model version 5.1, who noted that the tropical Indian Ocean is the main moisture source of the southern TP in summer. A subsequent quantitative study conducted by Zhang et al.

(2019) revealed that the water vapor transport originating from the Indian Ocean and Indochina to the TP contributes 51.4% of the precipitation moisture on the southern TP. Compared with the Eulerian method, the Lagrangian approach shows unique advantages in tracking water vapor, which can intuitively reveal moisture sources (Stohl and James, 2004; Stohl et al., 2005). Based on Lagrangian simulations, Huang and Cui (2015) pointed out that the majority of water vapor affecting extreme precipitation in the Sichuan Basin originates from the Sichuan Basin, the Bay of Bengal and the South China Sea. Chen and Xu (2016) further demonstrated that although the long-distance water vapor transport from the Bay of Bengal and the Arabian Sea contributes considerably to heavy precipitation in the Sichuan Basin, the most influential factor is the moisture from the Sichuan Basin and the surrounding region, as well as the South China Sea. It can be found that moisture sources differ between the precipitation on the southern TP and that in the Sichuan Basin. However, for the EPTP, a transition zone from the Tibetan Plateau to the Sichuan Basin, there have been relatively few studies on the quantitative identification of moisture sources in this region.

The topography of the EPTP features an elevation gradient of more than 3000 m from the west to the east, and the adiabatic cooling due to orographic uplift can lead to an increase in relative humidity and precipitation (Sokol and Bližňák, 2009), indicating that the effect of terrain on the precipitation extremes over this region are not negligible (Ma et al., 2018; Tuel and Martius, 2022). Studies have shown that the effect of topography on precipitation varies with the scale of the terrain, and large-scale (sub-mesoscale within a few kilometers) topography tends to amplify (diminish) the effect on precipitation through mechanical (thermal) forcing (Kimura and Kuwagata, 1995; Nishizawa et al., 2021). As early as the 1980s, Wang and Isidoro (1987) indicated that the blocking of topography on the eastern side of the TP favors the establishment of an unstable environment, and the terrain may dramatically affect the triggering of vortices through thermal forcing (Smith, 1989). It was also found that the mesoscale feature (30-120 km) of the topography plays an important role in generating and enhancing mesoscale disturbances over the TP (Shi et al., 2008). More importantly, the steeply sloping terrain of the EPTP also acts as a direct physical barrier to the movement of water vapor. Blocked by the steep topography, water vapor from the south moves northward along the narrow channel between the TP and the WPSH, converging with cold air from the north to generate heavy precipitation in the Sichuan Basin (Qian et al., 2022). Due to the noticeable amplifying effect of large-scale complex terrain on precipitation, the variation of precipitation with terrain height is more pronounced during the warm season over the EPTP (Hu et al., 2021). Despite the well-accepted influence of topography on precipitation, the effects on the relationship between precipitation and steep terrain in the EPTP remain poorly understood. In order to fully appreciate the effect of steep terrain on persistent Extreme precipitation (PEP) events over the EPTP, it is crucial to understand the individual mechanism. In particular, it is necessary to broaden our understanding of the influence of steep terrain under mechanically forced uplift and thermally driven circulation.

Considering the aforementioned factors, this study aims to address the following questions. What are the anomalous characteristics of the large-scale circulations during the occurrence of PEP events in the EPTP, and what role did they play in maintaining Extreme precipitation? What are the anomalies of water vapor transport during PEP events? How does the steep terrain contribute to the triggering, enhancement and duration of PEP events? Our motivation is to deepen our understanding of the combined effects of multiple factors (large-scale circulations, water vapor transport and steep terrain) on the PEP events in the EPTP.

The remainder of this paper is organized as follows. Section 2 presents the data, methods and model configuration. Section 3 analyzes the spatiotemporal characteristics of the PEP events and the associated climatological circulation patterns (Section 3.1), investigates the anomalies of moisture sources (Section 3.2) and discusses the effect of steep terrain (Section 3.3). Finally, Section 4 presents the main conclusions and discussion.

Table 1
Persistent Extreme precipitation events over the eastern periphery of the Tibetan Plateau during 1980–2021. Note that a total of 60 events are selected and utilized for the study, but only 18 events involving 3 or more stations are shown in this table.

Year	Date	Stations (duration)	Accumulated rainfall (mm)
1980	6.28–6.30	3 (3)	740.7
1980	7.27–7.29	3 (3)	442.2
1983	7.28–7.30	4 (3)	637
1984	7.11–7.13	4 (3)	565.2
1984	8.17–8.19	3 (3)	342.6
1987	6.24–6.27	3 (4)	605.4
1988	8.11–8.15	3 (5)	749.2
1990	8.26–8.28	3 (3)	415.8
1992	7.24–7.29	4 (6)	788.4
1998	7.4–7.6	5 (3)	1070.2
2007	8.29–8.31	5 (3)	739.4
2012	7.15–7.18	4 (4)	762
2013	6.18–6.21	3 (4)	618.4
2013	7.8–7.13	11 (6)	3720.4
2018	7.9–7.12	3 (4)	1068
2018	7.14–7.17	4 (4)	738.5
2019	8.19–8.23	7 (5)	1620.1
2020	8.15–8.18	22 (4)	6649.6

2. Data, model and methods

2.1. Datasets

The study region, EPTP (Fig. 1a), is confined to the domain of 29.8°N–31.5°N, 102.6°E–104.5°E. The PEP events are identified by using the daily precipitation data from 26 selected gauge stations located in the study region (Fig. 1c) in the summertime (June, July and August) from 1980 to 2021, which was released by the National Meteorological Information Center (NMIC) of the China Meteorological Administration (http://data.cma.cn/). In addition, the 0.25° × 0.25° CN05.1 gridded observation dataset provided by the NMIC (Wu and Gao., 2013; Jia et al., 2017) is utilized to offer a finer depiction of the spatial distribution of precipitation (Fig. 1b). Moreover, this dataset serves as the reference data to assess the accuracy of the simulations from the Weather Research and Forecasting Model (WRF), as shown in Fig. 9c.

The values of atmospheric variables, namely geopotential height, potential vorticity, air temperature, three-dimensional wind speed, specific humidity, column-integrated water vapor flux and divergence, are directly derived from the fifth-generation European Center for Medium-Range Weather Forecast atmospheric reanalysis of the global climate (ERA5; Hersbach et al., 2020; https://www.ecmwf.int/en/forecasts/dataset/ecmwf-reanalysis-v5). The spatio-temporal resolutions of the ERA5 product are 0.25° × 0.25° and 6 h (00:00, 06:00, 12:00, 18:00), and the vertical levels of this dataset are 37 levels from 1000 hPa to 1 hPa.

2.2. Definition of persistent Extreme Precipitation (PEP) events

Due to the differences in geography and surface conditions, it is not appropriate to define Extreme precipitation using a uniform criterion across different subregions of China (Wang et al., 2011). In this study, based on the local standard of Sichuan Province, the 24-h accumulated rainfall of 25 mm is taken as the Extreme precipitation threshold in the EPTP. If the daily precipitation at a station reaches 25 mm and this condition lasts for 3 days and longer, this precipitation event is considered as a PEP event. According to this criterion, a total of 60 PEP events within the study area during 1980–2021 are selected for research (Table 1).

Table 2
The configuration of the Weather Research and Forecasting Model (WRF) in this study.

Domain	D01	D02
Center point of the domain	30°N, 102.5°E	
Grid resolution	15 km	3 km
Unstaggered grid points	296 × 336	371 × 506
Short-wave radiation scheme	Dudhia scheme	Dudhia scheme
Long-wave radiation scheme	rapid and accurate radiative transfer model scheme	rapid and accurate radiative transfer model scheme
Microphysics scheme	WRF-single-moment-6-class scheme	WRF-single-moment-6-class scheme
Planetary boundary layer scheme	Yonsei University scheme	Yonsei University scheme
Cumulus parameterization scheme	Kain-Fritsch scheme	No
Surface layer scheme	Revised MM5 (Mesoscale Model version 5) Monin-Obukhov scheme	Revised MM5 Monin-Obukhov scheme
Land-surface scheme	Noah	Noah

2.3. Mesoscale numerical model and its configuration

This study uses the mesoscale numerical model, WRF version 4.0, to investigate the effects of steep topography along the southeastern margin of the TP on the PEP in the EPTP region, especially on water vapor transport and circulation anomalies. For this purpose, a control experiment is conducted to depict precipitation under initial topographical conditions. Additionally, five sensitivity experiments are implemented to gradually increase the initial topographical height of the basin up to a factor of six and investigate the corresponding precipitation response (Fig. 9b). To avoid integration non-convergence caused by topographic alteration, we transition the southern and eastern boundaries of the modified area along a gradient toward the surrounding 24 km (equivalent to 8 grid points).

The initial field and lateral boundary conditions of the model are obtained from the 1° × 1° Final Operational Global Analysis datasets provided by the National Centers for Environmental Prediction, which consist of 27 layers in the vertical direction and have a temporal resolution of 6 h (https://rda.ucar.edu/datasets/ds083.2/). The topographic input of the model is derived from the static geographic dataset embedded in the WRF (https://www2.mmm.ucar.edu/wrf/users/download/get_sources_wps_geog. html), and the CN05.1 gridded observation dataset from the NMIC is used as the precipitation observations to assess the reliability of the precipitation simulations. The simulation period is from 06:00 on August 14, 2020 to 06:00 on August 19, 2020, the model domain adopts two one-way nested grids, and an integration step is 60 s. The results are outputted hourly, with 39 vertical layers, including physical quantities such as three-dimensional wind field, water vapor flux, geopotential height, convective available potential energy (CAPE) and potential vorticity, all of which are used to reveal the dynamic and thermal effects caused by the terrain. The model configuration and setup of the physical parameterization schemes for the simulation in both domains refer to Yang et al. (2022), as shown in Table 2. It is worth noting that the cumulus convection parametrization scheme is primarily designed to describe the convection at a sub-grid scale. However, the resolution of 3 km × 3 km is smaller than the coverage range of most cumulus convection, and thus convection is no longer a sub-grid-scale phenomenon. Therefore, the cumulus convection scheme is not taken into account in the inner domain.

2.4. Lagrangian approach for moisture source identification

Actually, there are several models based on the Lagrangian method that can be used to research the trajectories and tracks of air parcels, such as the hybrid single-particle Lagrangian integrated trajectory model (Draxler and Hess, 1998) developed by the NOAA, the flexible particle dispersion (FLEXPART) model (Stohl and James, 2004; Stohl et al., 2005) and the Lagrangian analysis tool (Sprenger and Wernli, 2015). The FLEXPART has a unique “domain filling” technique embedded in the model, and the high-resolution output fields are suitable for a case study on airflows related to specific synoptic situations (Pisso et al., 2019). In recent decades, the FLEXPART has been widely used to investigate the atmospheric hydrological cycle, particularly for the determination of moisture sources/sinks (Sodemann et al., 2008; Chen and Li, 2021; Chen et al., 2018b; Gimeno et al., 2012; Sun and Wang, 2014; Drumond et al., 2019; Liu et al., 2022). ERA-Interim reanalysis data (60 hybrid model levels from the surface to 0.1 hPa, 0.75° × 0.75° longitude/latitude grid resolution and 6-h temporal resolution) are applied to drive the Lagrangian transport model FLEXPART.

In this study, we initially divide the three-dimensional space of the region (from 20°N to 60°N and from 0°E to 160°E) into approximately 1.4 million air parcels based on the domain-filling technique, and the integration period is from May 1, 1980 to August 31, 2017. Considering a 10-day water vapor circulation cycle (Trenberth, 1998, 1999), we trace the air parcel groups backward for 1–10 days to gain insight into their atmospheric transport processes. The outputs are recorded at a 6-h interval, providing information on the three-dimensional coordinates (latitude, longitude and altitude) of air parcels and the physical quantities such as temperature, specific humidity and mass. However, for the moisture source diagnosis, only those air parcels residing or reaching whole column atmosphere over the target region during the modelling period are selected and then traced backward for ten days.

To identify the evaporative moisture sources, the Lagrangian moisture source diagnosis method proposed by Sodemann et al. (2008) is further employed. This method takes into account the variation of specific humidity during the motion of air parcels along their trajectories, i.e., evaporation processes increase the specific humidity, while precipitation decreases the specific humidity of the air parcels. This allows the determination of the source-sink region along the water vapor transport path. Eventually, the evaporative fields from all trajectories are linearly interpolated onto a regular 1.0° × 1.0° grid to construct the 38-year climatology of well-resolved 6-h trajectory-based moisture source fields in the EPTP that allows us to explore the spatio-temporal variabilities and their association with PEP events.

2.5. Thermal-dynamical diagnosis method

In this study, the definition of equivalent potential temperature (Eq. 1) proposed by David (1980) is used to analyze the warm and moist conditions of air masses.

$$\theta_E = T_K\left(\frac{1000}{p}\right)^{0.2854\left(1-0.28\times10^{-3}r\right)} \times exp\left[\left(\frac{3.376}{T_L}-0.00254\right)\times r\left(1+0.81\times10^{-3}r\right)\right] \quad (1)$$

where $T_K(K)$, $p(hpa)$ and $r(\%)$,represent the absolute temperature, air pressure and mixing ratio at the initial height, respectively, and T_L(K), denotes the absolute temperature at the lifting condensation level calculated by the relative humidity.

The horizontal wave activity flux W_{2d} (Koutarou and Hisashi, 2001) is used to diagnose the propagation of quasi-stationary waves in the atmosphere and is calculated by Eq. (2).

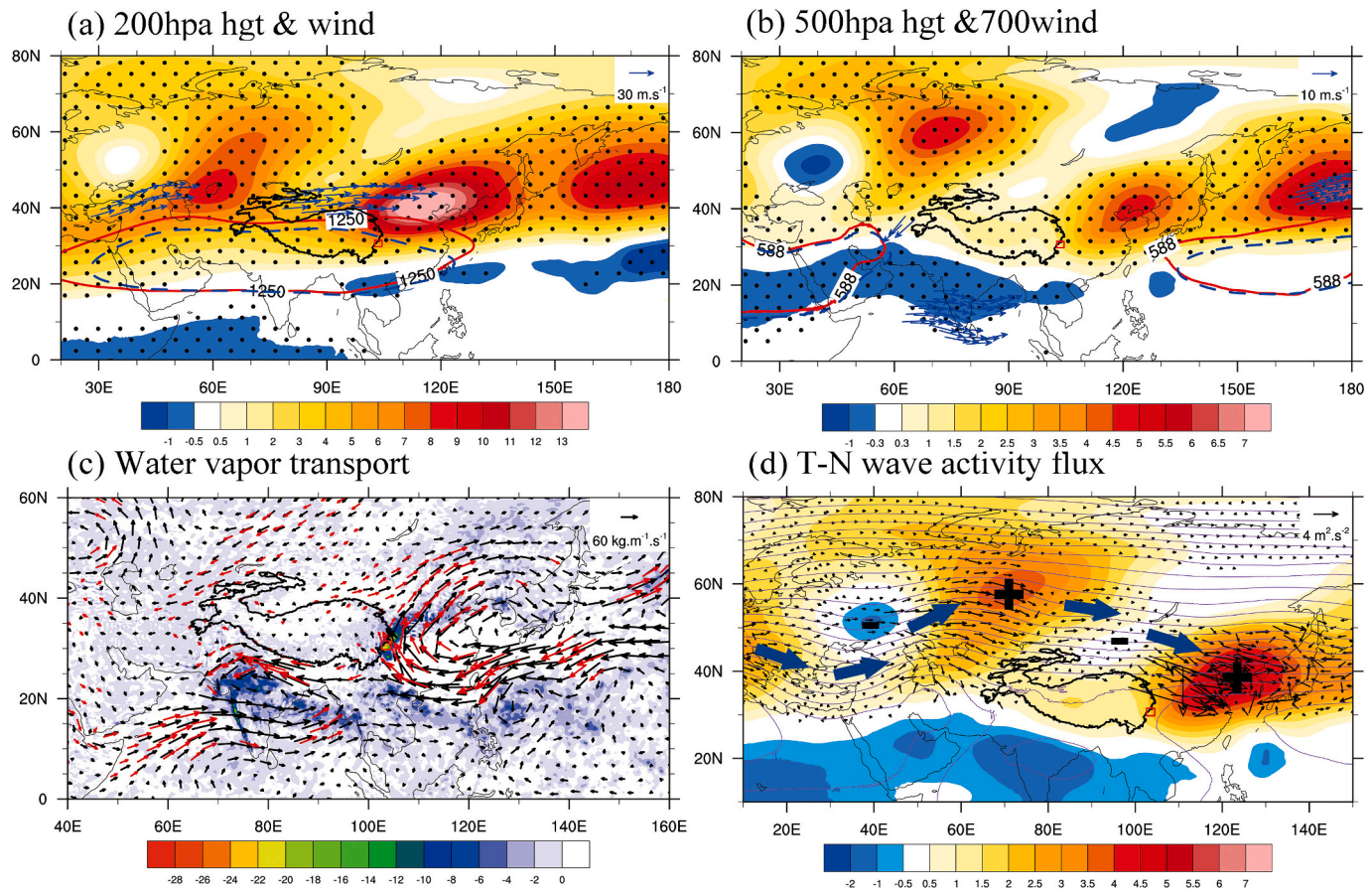

Fig. 2. (a) The composite fields of the geopotential height anomaly (color shaded areas, dagpm), westerly jet stream (vector, exceeding 30 m s^{-1}, m s^{-1}) and the evolution of the South Asian high (SAH) at 200 hPa, (b) the composite fields of the geopotential height anomaly (color shaded areas, dagpm), the evolution of the western Pacific subtropical high (WPSH) at 500 hPa, and the low-level jet (vector, exceeding 12 m s^{-1}) at 700 hPa, (c) the distribution of the water vapor transport anomaly, and (d) the distribution of the T-N wave activity flux (vector) at 500 hPa during the PEP events over the EPTP. In Fig. 2a, the blue dashed line represents the climatic state, and the red solid line indicates the composite during the PEP events. In Fig. 2b, the blue dashed lines represent the climatic state, and the red solid line indicates the composite during the PEP events. In Fig. 2c, the vector indicates the integrated water vapor flux, and the shaded areas represent integrated water vapor flux divergence. In Fig. 2d, the shaded areas present the stream function anomaly, the solid purple contours represent the original geopotential height at 500 hPa. Note that the climatic state for this study adopts the summer mean during the period of 1980–2021. Black dots in (a) and (b) and red arrows areas in (c) show the geopotential height and water vapor anomalies, respectively, that are significant at the 95% confidence level based on a *t*-test. (For interpretation of the references to color in this figure legend, the reader is referred to the web version of this article.)

$$W_{2d} = \frac{pcos\phi}{2|U|}\left(\begin{array}{cc} \frac{U}{a^2cos^2\phi}\left[\left(\frac{\partial\psi'}{\partial\lambda}\right)^2 - \psi'\frac{\partial^2\psi'}{\partial\lambda^2}\right] + \frac{V}{a^2cos\phi}\left[\frac{\partial\psi'}{\partial\lambda}\frac{\partial\psi'}{\partial\phi} - \psi'\frac{\partial^2\psi'}{\partial\lambda\partial\phi}\right] \\ \frac{U}{a^2cos\phi}\left[\frac{\partial\psi'}{\partial\lambda}\frac{\partial\psi'}{\partial\phi} - \psi'\frac{\partial^2\psi'}{\partial\lambda\partial\phi}\right] + \frac{V}{a^2}\left[\left(\frac{\partial\psi'}{\partial\phi}\right)^2 - \psi'\frac{\partial^2\psi'}{\partial\phi^2}\right] \end{array}\right) + C_U M \quad (2)$$

where ψ' represents the perturbation stream function, $|U|$ the horizontal wind speed and p the pressure divided by 1000 hPa. C_U is the vector that represents the phase propagation in the direction of U.

$$C_U = C_p\frac{U}{|U|} = \left(\frac{U}{|U|}C_P, \frac{V}{|U|}C_P, 0\right)^T$$

M is the wave-activity (angular) pseudomomentum, which defined as:

$$M = \frac{p}{2}\left(\frac{q'^2}{2|\nabla_H Q|} + \frac{e}{|U| - C_p}\right)cos\phi$$

The climatic state during the summer of 1980–2021 is chosen as the background field. Since the monthly average value of C_UM is small, it will be ignored in the calculations in this paper.

3. Results

3.1. Spatio-temporal characteristics of PEP events and the configuration of associated large-scale circulation systems

Fig. 1b shows the distributions of the climatic average rainfall amounts during the summer of 1980–2021 and 60 PEP events (comprising a total of 207 days of Extreme precipitation) identified by the algorithm presented in Section 2.2. The rain belt of summer mean precipitation on the southeastern side of the TP is located in the south, with a high-value center of 8.8 mm d^{-1}. However, the maximum rainfall amount exceeds 30 mm d^{-1} during the PEP events, and the precipitation center shows a northward shift (Fig. 1b). The frequency of PEP events is consistent with the rainfall distribution of PEP events, with a total of 1–30 occurrences over 40 years. Specifically, our study area, EPTP, experienced both the highest frequency and greatest amount of persistent precipitation (Fig. 1c). At an interannual scale, the evolution of both factors (the frequency and rainfall amount of PEP events) remains consistent (Fig. 1d). It is noteworthy that the frequency of PEP events in the EPTP shows a marked increasing trend over the last 20 years (after

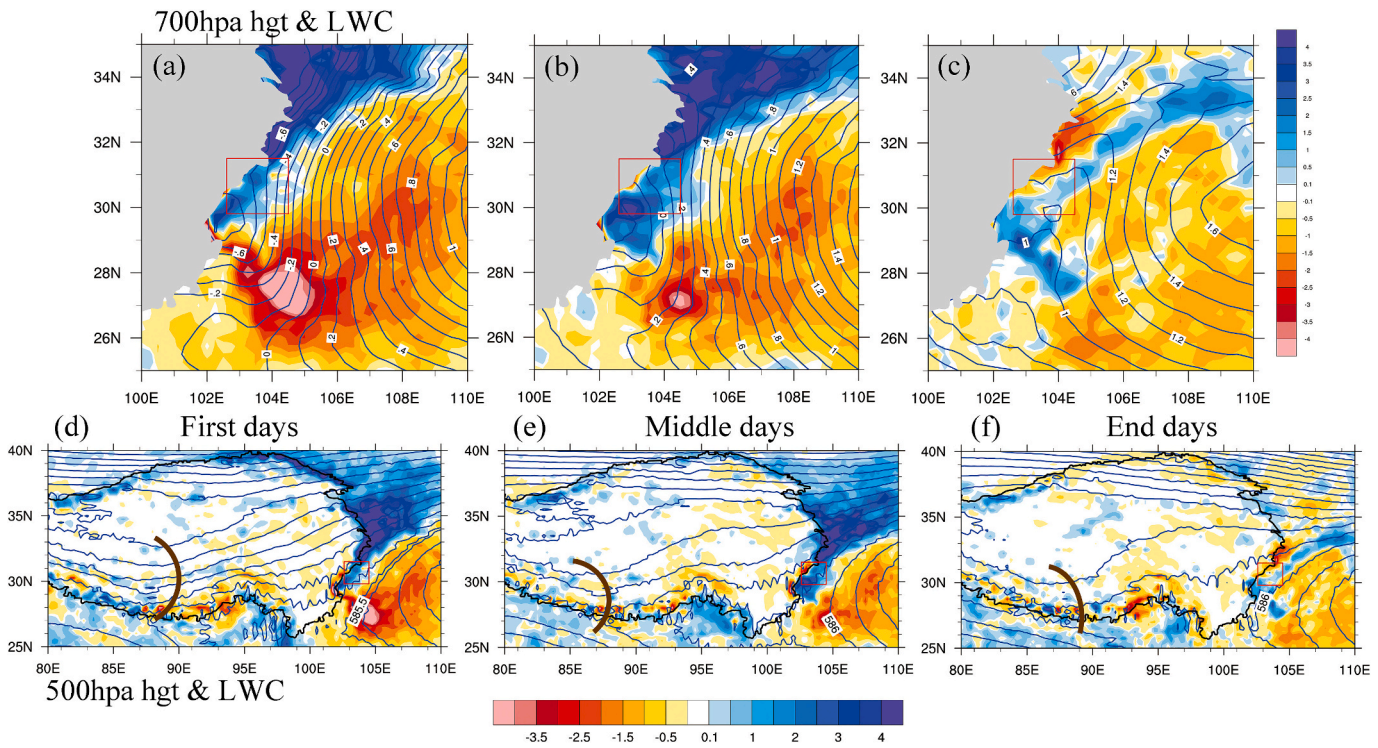

Fig. 3. The composites of the geopotential height anomaly (contours, dagpm) and liquid water content (color shaded areas, 10^5 kg kg^{-1}) at (a–c) 700 hPa and (d–f) 500 hPa in (a and d) the first days, (b and e) the middle days and (c and f) the end days during the PEP events over the EPTP.

2000).

In order to identify the atmospheric circulation responsible for the PEP events over the EPTP, we composite the geopotential height and wind fields during the same periods of the PEP events, as shown in Fig. 2, to investigate the corresponding anomalous circulation patterns. The results indicate that during the PEP events, the South Asian high (SAH) covered almost the entire TP, and the EPTP was located to the northeast of the SAH and within the exit zone of the westerly jet (Fig. 2a), leading to more favorable upper-level divergence conditions (Wang and Ho, 2002; Samel, 2003). More importantly, during the PEP events, the SAH extended northward and eastward (Fig. 2a), and the WPSH extended northward and westward (Fig. 2b), accompanied by the pronounced southwest low-level jet stream along the Arabian Sea-Bay of Bengal (Fig. 2b). This relative change in the WPSH and SAH facilitates the

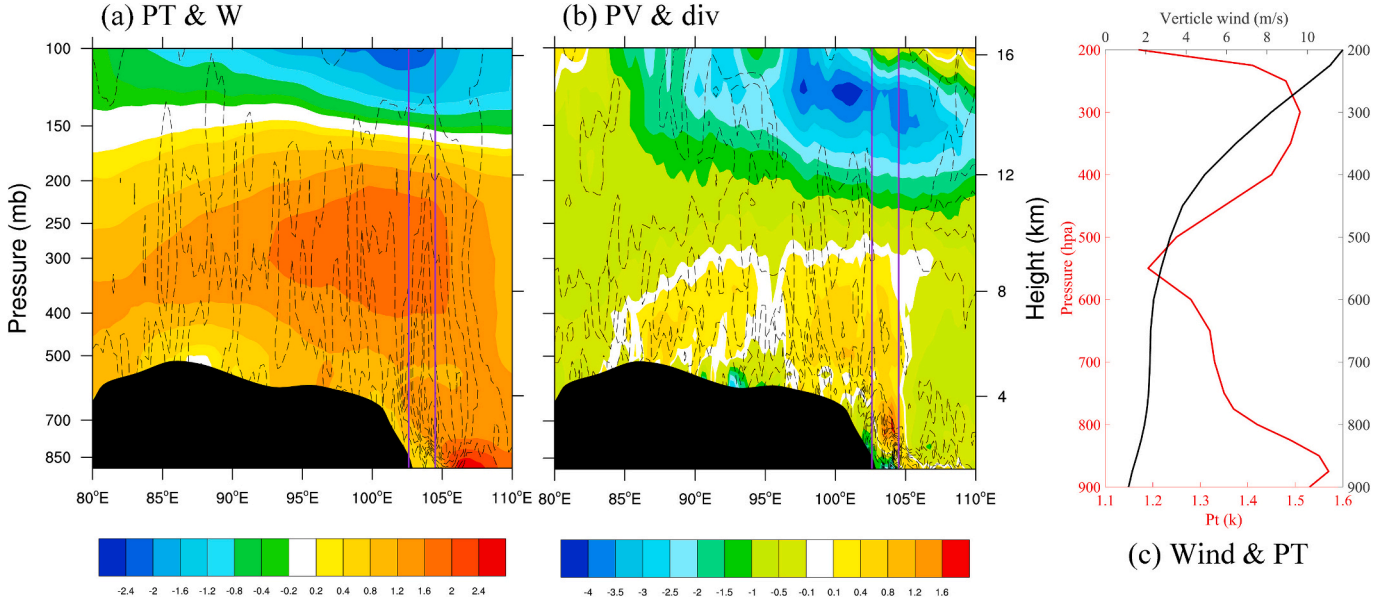

Fig. 4. (a) Vertical distribution of the composited potential temperature anomaly (color shaded areas, K) and vertical velocity (dashed contours with values below zero, Pa s^{-1}), (b) vertical distribution of potential vorticity anomaly (color shaded areas, 10^7 K m^2 kg^{-1} s^{-1}) and divergence (dashed contours with values below zero, s^{-1}) during the PEP events, (c) the vertical profiles of the potential temperature anomaly (red lines) and wind anomaly (black lines) over the EPTP. Note that in Fig. 4a and b, the latitudinal mean values are calculated between 28°N and 32°N, and the area enclosed by the solid purple line represents the EPTP. (For interpretation of the references to color in this figure legend, the reader is referred to the web version of this article.)

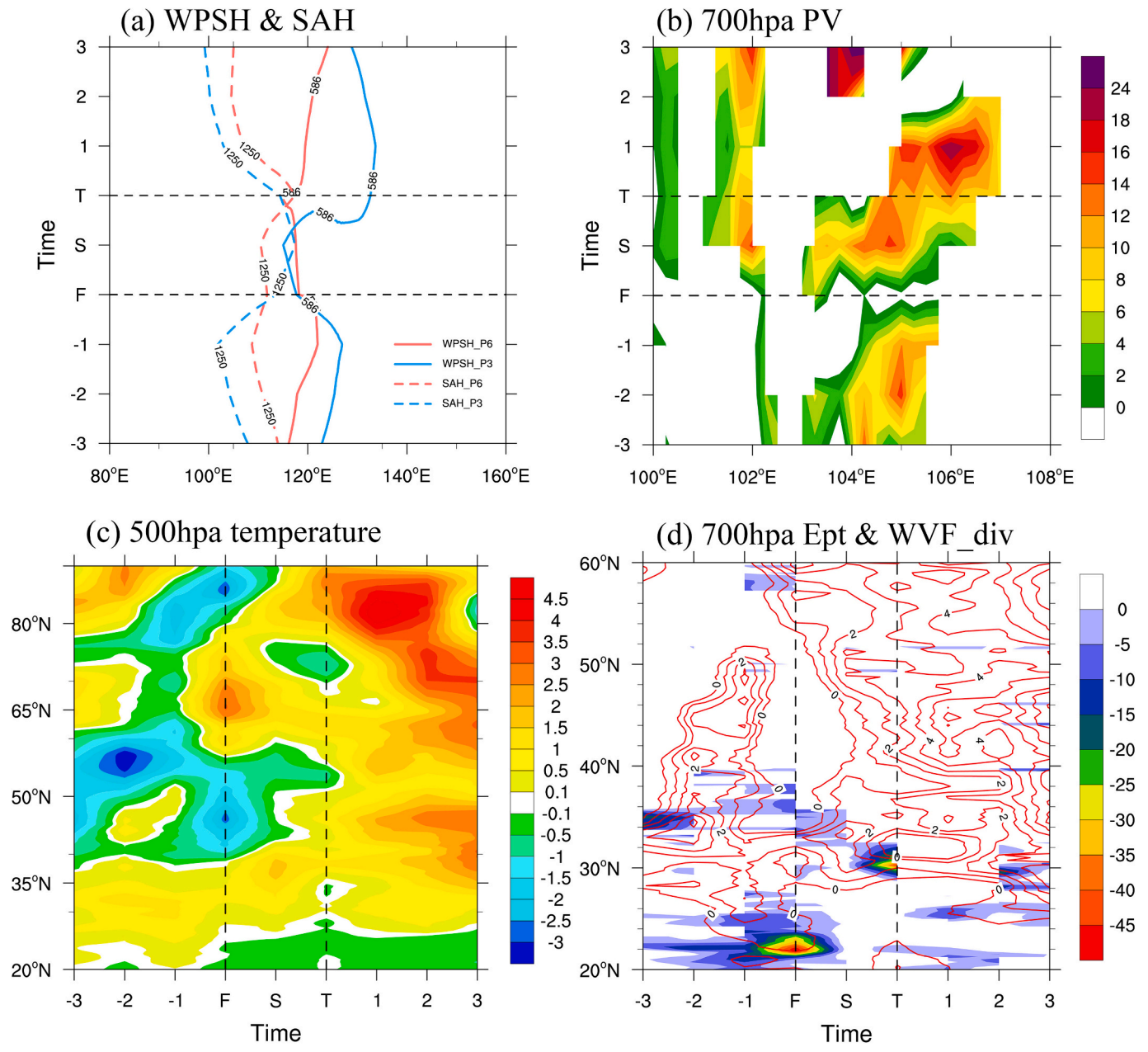

Fig. 5. (a) Time-longitude profiles of the spatial distribution in the WPSH and the SAH (We use 586 dagpm and 1250 dagpm to represent WPSH and SAH, respectively.), (b) time-longitude profiles of the differences in 700 hPa potential vorticity, (c) latitude-time profile of the differences in 500 hPa temperature, and (d) latitude-time profiles of 700 hPa equivalent potential temperature (red solid lines) and water vapor flux divergence (color shaded areas). In Fig. 5a, the range of the WPSH averaged along the zonal direction is 0°N–40°N, while that of the SAH averaged along the zonal direction is 15°N–40°N. Note that the differences are calculated as the P6 type minus the P3 type, and the rectangular dashed boxes indicate the period of PEP events. (For interpretation of the references to color in this figure legend, the reader is referred to the web version of this article.)

effective transport of warm and humid airflows from the southern region to the EPTP (Zhou and Wang, 2019), which coincides with the findings of Xu et al. (2014).

The geopotential height anomaly field maintains a similar distribution of positive-negative phases from 700 hPa to 200 hPa (the geopotential height anomaly at 700 hPa is omitted), i.e., an equivalent barotropic structure with a "negative-positive-negative-positive" pattern from the west to the east at mid- and high-latitudes. The 500 hPa wave train-like structure is the most apparent, with a positive geopotential height anomaly region over the Northeast Asian coast, a positive anomaly region to the north of the Sea of Okhotsk, and a negative anomaly region in the Lake Baikal between them (Fig. 2b). The distribution of mid-latitude geopotential height anomaly field favors the southward movement of dry and cold air along the trough. When the dry and cold air converges with the northward-moving warm and moist air, the meridional gradients of temperature and specific humidity are enhanced, thus benefiting the occurrence and persistence of precipitation events. Further calculations of the T-N wave activity flux reveal that the mid- and high-latitude wave trains, guided by the westerly jet stream, spread energy from the west to the east, and thus, there is a positive region of stream function and a large-value region of wave activity flux in Northeast Asia (coinciding with the positive geopotential height anomaly areas). The energy accumulation triggers the formation of an anomalous anticyclonic system in Northeast Asia (Fig. 2d).

Under the impact of this anomalous anticyclone, pronounced anticyclonic water vapor convergence anomalies are observed over the

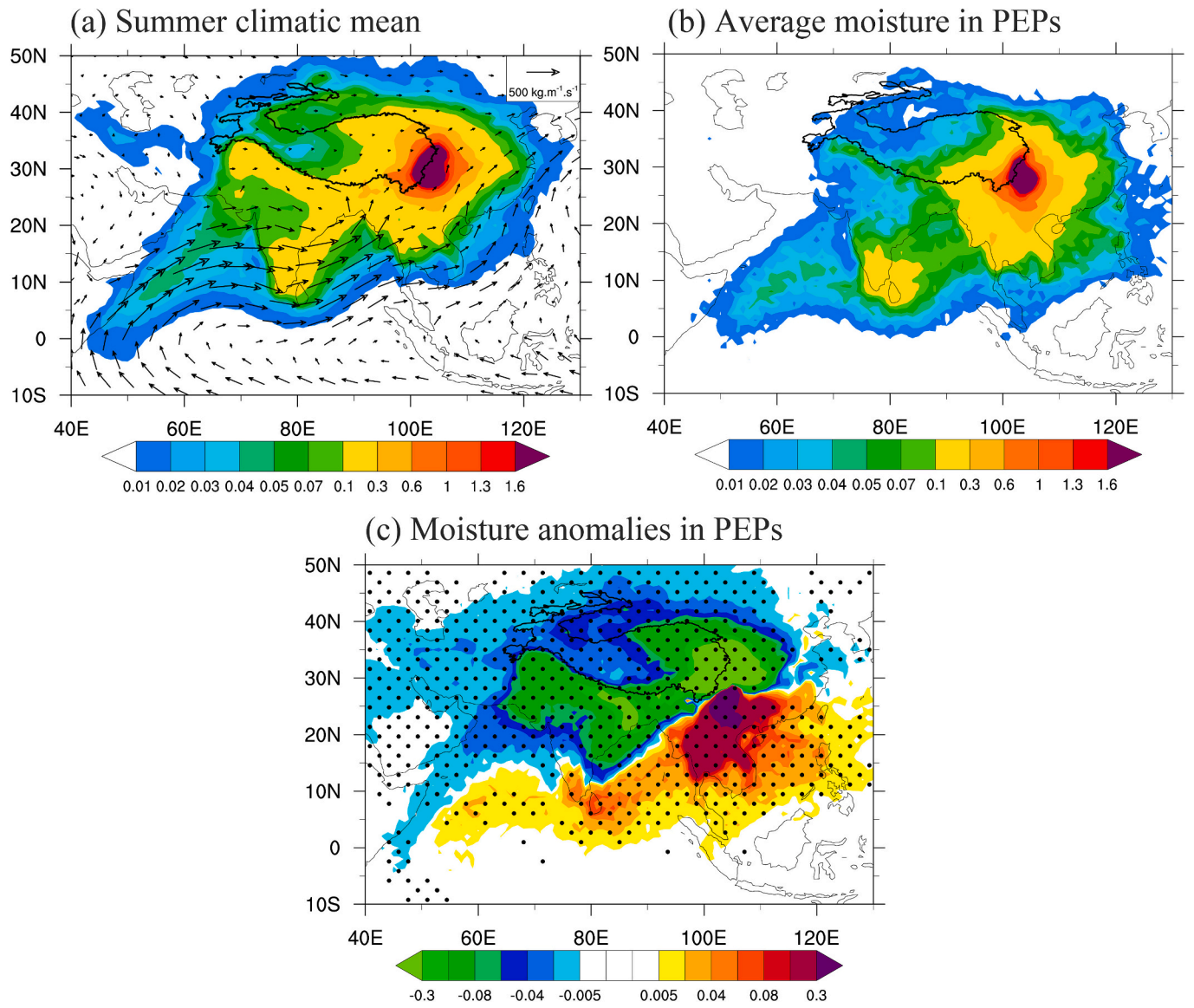

Fig. 6. Lagrangian moisture sources during (a) the summer climatic state (color shaded, mm d^{-1}, the vector represents the integrated water vapor flux (kg m^{-1} s^{-1}) during the same period.) and (b) the PEP events, (c) moisture source anomalies during the PEP events (mm d − 1). Note that the climatic state in this study is taken as the summer mean for the period 1980–2021. Black dots in (c) indicates the composite moisture sources difference between the climate state and that of PEP events are significant at the 95% confidence level based on a *t*-test.

EPTP during the PEP events, which, in conjunction with the westward extension and northward movement of the WPSH (Yang et al., 2010; Ren et al., 2015), facilitates more moisture transport from the eastern ocean to the EPTP (Fig. 2c). Additionally, during the PEP events, there is substantial southwesterly water vapor transport originating from the Arabian Sea-Bay of Bengal, highlighting the contribution of southwestward moisture transport to the PEP events under the influence of the South Asian monsoon. The contribution of moisture source subregions to the PEP events in the EPTP is examined in detail in Section 3.2.

Influenced by the eastward extension of the SAH and the westward extension of the WPSH, the EPTP is always located in front of the southern branch trough during the PEP events, and the precipitation processes are accompanied by the eastward propagation of small perturbations (Fig. 3d–f). In the lower levels, the EPTP is obviously influenced by a southwest vortex system, and the study area remains under the control of the low-pressure system. The liquid water content shows a north-south dipole structure on the eastern side of the plateau, with positive anomaly areas in the center of the southwest vortex and its northeastern band and negative anomaly areas over the majority of the southeastern region (Fig. 3a–c). The convergence in front of the trough strengthens the southwest vortex system and facilitates the convergence and concentration of the water vapor. This condition, coupled with the stratification instability caused by the convergence of the cold and warm advection due to geopotential height anomaly, intensifies the upward motion, which in turn is more conducive to the development of mesoscale convective systems and the persistence of precipitation.

The potential temperature anomaly of the atmosphere during the PEP events shows an unstable structure in the troposphere, with warm lower layers and cold upper layers, characterized by upward motion (Fig. 4a). The vertical profile of the potential temperature indicates that it decreases with height below 550 hPa (Fig. 4c), suggesting that compared with the ambient air, the air mass has higher internal energy, higher temperature and lower density at this point, and thus leading to intense upward motion. The potential vorticity also exhibits positive anomalies during the PEP events (Fig. 4b). According to the energy conservation law of potential vorticity, an increase in potential vorticity can lead to the vertical stretching of air columns, thus enhancing cyclonic rotation. In conjunction with the convergence at lower levels

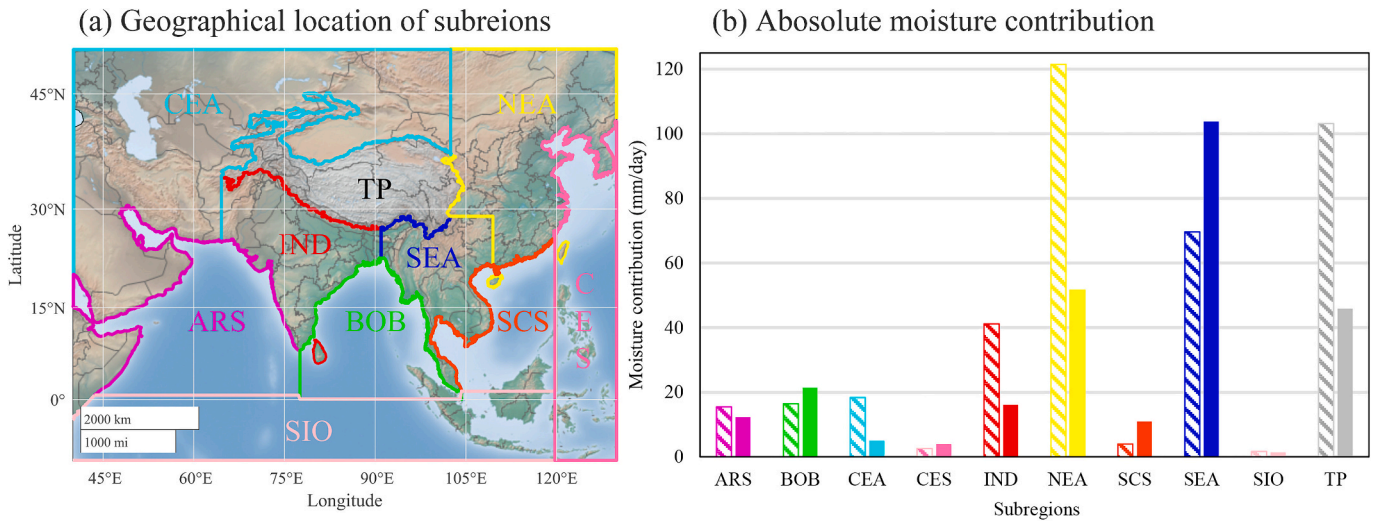

Fig. 7. (a) The distribution of the 10 different subregions of moisture sources (The Arabian Sea (ARS), Bay of Bengal (BOB), Central Eastern Asian(CEA), Eastern China Sea(CES), Indian continent(IND), Northeastern Asian(NEA), Southern China Sea(SCS), Southeastern Asian(SEA), South Indian Ocean(SIO), Tibetan Plateau (TP)). (b) Moisture contribution (*mm/day*, the colors of the bars in the figure match the colors of the subregions in Fig. 7a.) to EPTP summer precipitation in PEP (Solid color fills) and climatic mean (pattern fills).

and the enhancement of vertical wind, the increase of potential vorticity is highly conducive to the development of convection.

To clarify the influence of large-scale circulations on the duration of Extreme precipitation, we further subdivided the PEP events into two types of sub-events with durations of 3 days (P3) and 6 days (P6), and the changes of the physical quantities before and after the two types of sub-events are composited (Fig. 5). Both categories of sub-events are characterized by a westward extension of the WPSH and an eastward extension of the SAH, and these extensions intersect during PEP events. However, for the P6 type, the westward extension of the WPSH and the eastward extension of the SAH is more pronounced, and the zonal distance between the two systems is closer (Fig. 5a). Both categories of sub-events have obvious positive vorticity centers in the lower layers during the PEP events. Compared with the P3 type, the positive vorticity center of the P6 type appears three days prior to the precipitation and persists until three days after the precipitation (Fig. 5b). The positive vorticity center is usually accompanied by notable upward motion in front of the upper-level trough. This synoptic-scale system provides conditions or environmental fields for the formation of mesoscale weather systems, creating unstable stratification and convergence of low-level wind fields, which allows water vapor to converge in the rainstorm area (Luo et al., 2020). In terms of thermal conditions, for the P6 type, there is sufficient convergence of warm and cold air from higher to lower latitudes. This leads to an amplified meridional temperature gradient and facilitates the condensation of water vapor, thus promoting the occurrence of heavy rainfall (Fig. 5c). Further studies show that the P6 events correspond to higher equivalent potential temperature and stronger water vapor convergence (Fig. 5d), which reflects the fact that the atmospheric potential instability in the EPTP is highly favorable for the continuous triggering of convection in this region.

3.2. Moisture source anomalies of the PEP events over the EPTP

Fig. 6a presents the moisture sources during the summer climatic state and the PEP events, and the results show an overall southwest-northeast distribution of the summer climatic state of moisture sources in the EPTP, which is consistent with the direction of water vapor flux in the Eulerian framework. This distribution implies that the moisture supplying the summer precipitation in the EPTP is typically regulated by the Indian summer monsoon. The moisture sources encompass the South China Sea, the Bay of Bengal, the Arabian Sea and even the Indian Ocean

Table 3
Relative moisture contribution ratios of subregions in climatic mean and PEPs and their differences.

Percentage(%)	ARS	BOB	CEA	CES	IND
Climatic mean	3.94	4.17	4.67	0.65	10.45
PEPs	4.51	7.84	1.85	1.46	5.92
Difference	0.58	3.67	−2.82	0.81	−4.53
Percentage(%)	**NEA**	**SCS**	**SEA**	**SIO**	**TP**
Climatic mean	30.84	1.01	17.67	0.43	26.18
PEPs	18.93	4.03	38.1	0.5	16.86
Difference	−11.92	3.02	20.43	0.07	−9.32

to the south, and they cover the entire plateau and the parts of Central Asia to the northwest. To the east, these sources extend through the East Asian terrestrial region to the eastern seas of China, indicating the involvement of the East Asian summer monsoon in regulating water vapor transport. It is noteworthy that the high-value center of moisture sources is located on the southeastern side of the TP and is concentrated over the land areas, suggesting that local circulation processes in the Sichuan Basin and its surrounding regions also contribute notably to the PEP events in the EPTP (Chen and Xu, 2016). Simultaneously, we further composite the moisture sources of the PEP events in the EPTP and calculate their anomalies relative to the climatic state. The moisture sources extend further eastward and southward, stretching eastward across the South China Sea into the western Pacific and almost reaching the equator to the south (Fig. 6b).

In terms of moisture source anomalies, the moisture contribution from the southern Sichuan Basin-Indochina Peninsula and low-latitude oceans such as the South China Sea, the Bay of Bengal and the Arabian Sea is notably larger, while that from the mid- and high-latitude land areas, such as the TP and the Indian Peninsula, is considerably smaller (Fig. 6c). This is consistent with previous findings, i.e., Huang and Cui (2015) indicated that the moisture contribution from the Indian Peninsula-Bay of Bengal-Indochina Peninsula region had the greatest impact on extreme precipitation events in the Sichuan Basin. Chen and Xu (2016) further pointed out that although the moisture transport from the Arabian Sea-Bay of Bengal contributes substantially to Extreme precipitation events in the Sichuan Basin, the most influential factor is still the moisture contribution from the Sichuan Basin itself, as well as the Indochina Peninsula and the South China Sea region.

We further classify the moisture sources into ten sub-regions (Fig. 7a)

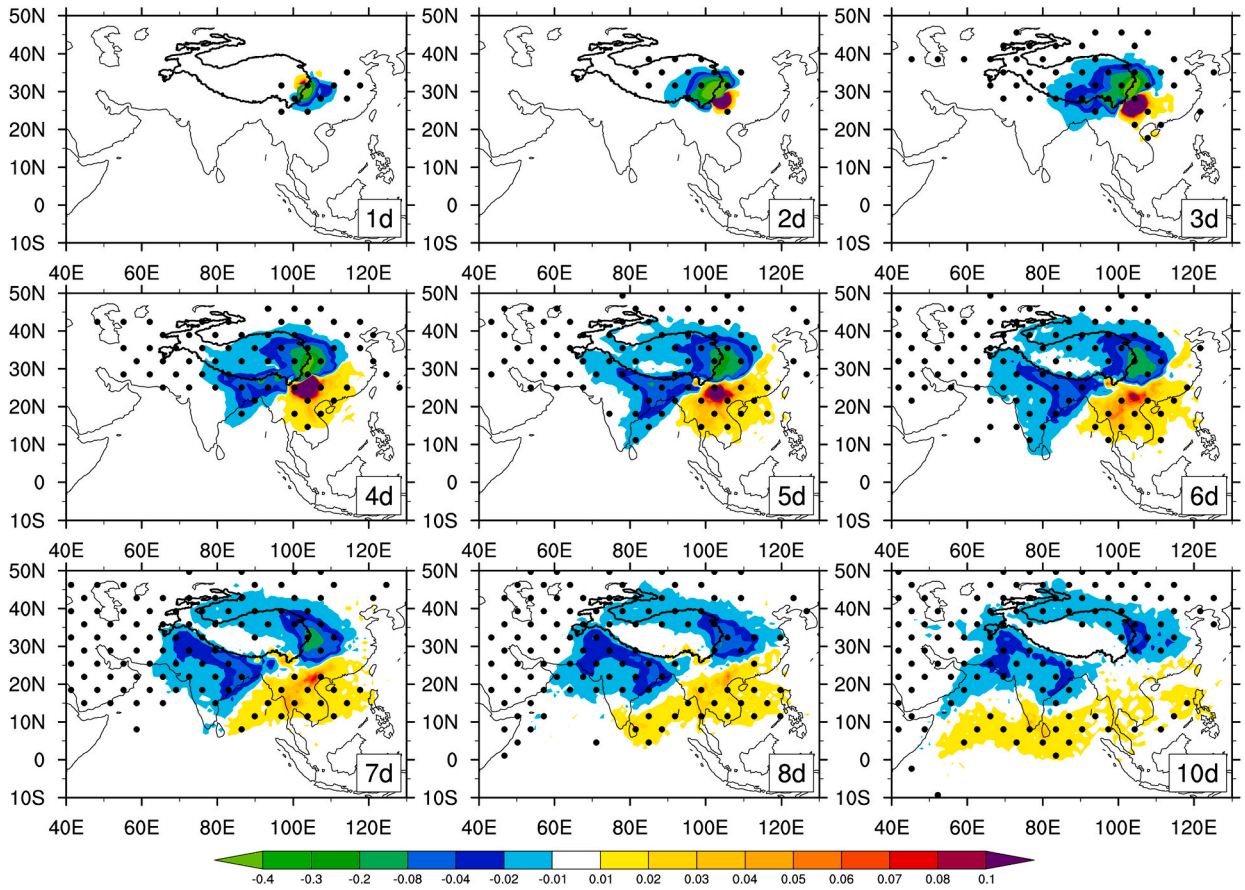

Fig. 8. Anomalous patterns of moisture tracked backward for 1–10 days over the EPTP in summer during the PEP events (mm d^{-1}). Black dots show the moisture anomalies during PEP are significant at the 95% confidence level based on a *t*-test.

and quantitatively assess their absolute (Fig. 7b) and relative contributions (Table 3) to water vapor. From the perspective of the average climatic state of moisture sources, the proportion of water vapor from Northeastern Asian (NEA) is the largest (30.84%), followed by the Tibetan Plateau (26.18%). However, during the PEP events in the EPTP, the largest proportion of water vapor (38.1%) comes from the Southeastern Asian (SEA), closely followed by NEA (18.93%). This result suggests that for the PEP events in the EPTP, the modulation of the East Asian summer monsoon plays a leading role in transporting water vapor to the EPTP through both the East Asia and South China Sea paths. In contrast, the SEA provides the majority of the water vapor for the PEP events, although NEA is the main contributor of moisture during the summer. In addition, the Indian (South Asian) summer monsoon (ARS, BOB and SCS) also contributes in a complementary way (16.38%). In general, the evaporative moisture sources from the SEA, BOB, and SCS are remarkably enhanced during PEP events, with a total contribution of 56.44%, which is 28.5% higher than the climatic mean.

To better visualize the process of water vapor transport to the EPTP, we further present the anomalous patterns of moisture tracked backward for 1–10 days during the PEP events (Fig. 8). As early as 10 days before the occurrence of precipitation, the supply of water vapor to the PEP events in the EPTP begins. The water vapor from the Arabian Sea-Bay of Bengal-Indochina Peninsula-South China Sea region is notably abundant on a longer time scale (7–10 days). The terrestrial moisture sources along the southern side of the Sichuan Basin-Indochina Peninsula region tend to exhibit positive anomalies on a shorter time scale (4–6 days), while the positive anomalies on a short time scale (1–3 days) are concentrated on the southern side of the Sichuan Basin. Notably, during the process of water vapor transport, the contribution of moisture from the entire plateau and land areas, such as the Indian Peninsula to the south, is obviously weaker, indicating that both the East Asian monsoon and the South Asian monsoon simultaneously regulate the PEP events in the EPTP. Therefore, it is more likely that water vapor originates from long-distance moisture transport from the ocean (the Bay of Bengal and the South China Sea), while water vapor from land areas such as the TP and the Indian Peninsula is relatively limited and predominantly apparent on shorter time scales.

3.3. *Effects of the steep terrain*

On August 15–18, 2020, a typical PEP event occurred, which lasted for 4 days and involved 22 meteorological stations in the study area. The accumulated rainfall reached nearly 7000 mm, resulting in urban waterlogging, landslides and severe economic losses. Whether in terms of precipitation extent, intensity or duration, this event can be regarded as a relatively rare PEP event. The event has been selected as one of the top ten natural disasters in China in 2020 by the Ministry of Emergency Management (https://www.mem.gov.cn/xw/yjglbgzdt/202101/t20210102_376288.shtml), drawing attention from scholars worldwide (Xia et al., 2021; Qian et al., 2022; Ma et al., 2022). Therefore, we conduct a simulation study on this weather process by using the mesoscale numerical model, WRF. To examine the role of steep terrain (red rectangular in Fig. 9a) in PEPs, a control experiment with equipped with original terrain and five sensitivity experiments with altered terrain are performed, and the parameterization schemes for physical processes used in the model are described in Section 2.3. In the sensitivity experiments, the terrain height in the red box is multiplied on a whole, and its zonal average reflects variation in terrain height (Fig. 9b). Before analyzing the simulated results, the performance of the WRF on precipitation characteristics is evaluated by taking the precipitation from

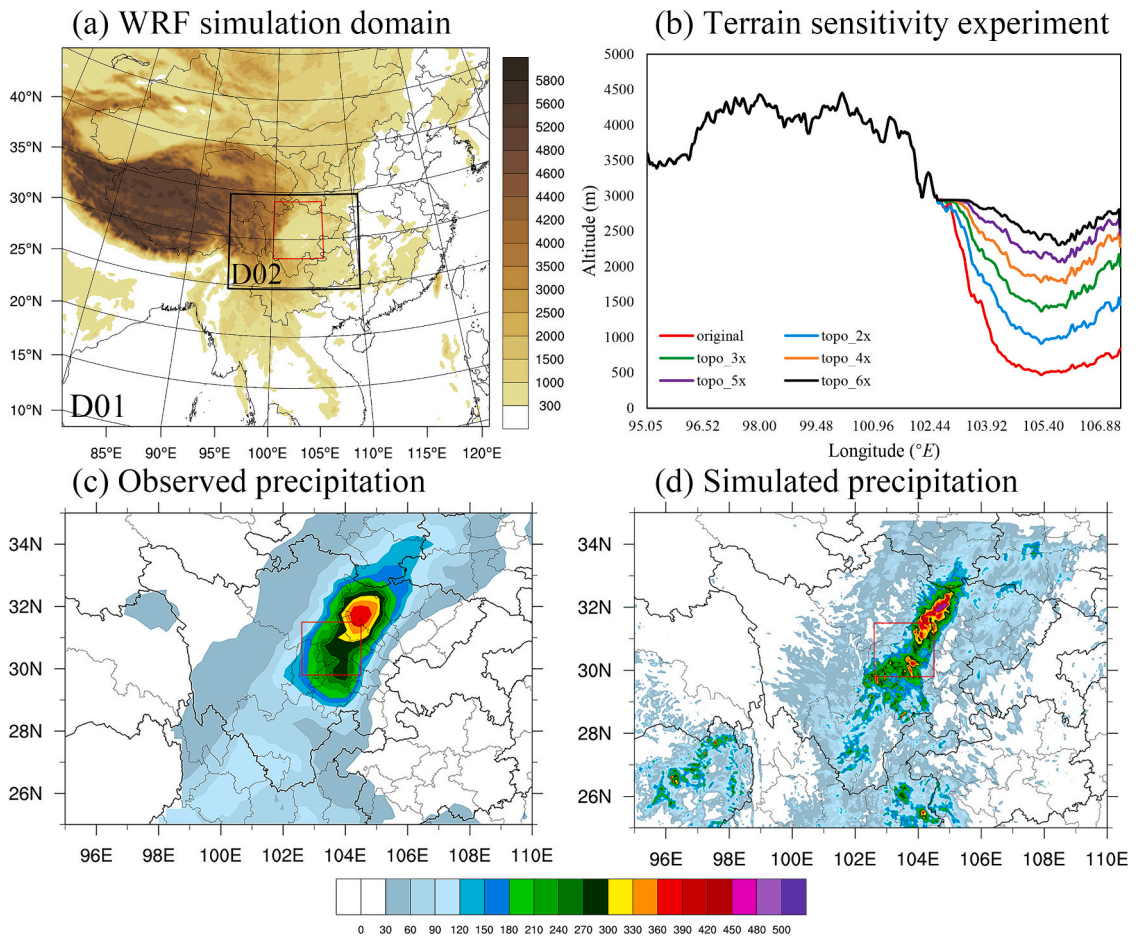

Fig. 9. (a) Terrain heights in the WRF simulation region D01 and nested region D02, (b) Zonally average topographic profile from the sensitivity experiment in the red rectangle of Fig. 9a where the terrain-filling simulation is performed, (c) accumulated rainfall from the CN05.1 dataset on August 15–18, 2020, and (d) accumulated rainfall simulated by the WRF control experiment (mm), the red rectangular in Fig. 9c and Fig. 9d indicates the EPTP. (For interpretation of the references to color in this figure legend, the reader is referred to the web version of this article.)

the CN05.1 dataset as the reference data (Fig. 9c). Although the precipitation is overestimated in the WRF control experiment, the simulations can better reproduce the southwest-northeast oriented rain belt in the Sichuan Basin and accurately capture the range and high-value center of precipitation (Fig. 9d).

The simulated precipitation in the target area gradually decreases with the increase of terrain height. When the terrain rises to 6 times the original height, there is almost no precipitation in the simulations (Fig. 10 a1–a5). To reveal the influence mechanism of the terrain slope on precipitation, we analyze several physical quantities of the WRF output. It can be found that the initial difference in terrain height corresponds to the better convergence of north-south airflow in the basin area. However, as the elevation of the basin rises, this convergence of meridional wind gradually disappears, and the airflow is blocked by the topography (Fig. 10 b1–b5). The terrain slope has a remarkable effect on the lower-level water vapor transport, i.e., the lifting of the terrain notably reduces the water vapor flux and correspondingly weakens the radar echo intensity. In contrast, the control experiment exhibits evident cyclonic water vapor convergence and strong echoes in the target area (Fig. 10 c1–c5), suggesting that the original difference in terrain height greatly favors the generation of convective cloud systems.

The CAPE and equivalent potential temperature are further calculated to provide a more intuitive assessment of the vertical atmospheric stability. The CAPE decreases with the topographic elevation. The CAPE differences between the control experiment and the sensitivity experiment reach the maximum when the terrain rises to 6 times the original terrain (Fig. 11 a1–a5), suggesting that the vertical atmosphere in the study area is unstable during the PEP events and convection is more likely to be triggered and develop under favorable warm and humid air conditions. The vertical distributions of potential temperature and water vapor mixing ratios further confirm this conclusion. From upper to lower levels, widespread positive potential temperature anomaly appears over the EPTP. Additionally, the control experiment shows more abundant water vapor content than the sensitivity experiment, further supporting the favorable warm and humid air conditions (Fig. 11 c1–c5). Therefore, our study suggests that the steep terrain places the EPTP in a warm and humid environment with highly unstable energy. The large terrain slope results in sufficient convergence of north-south airflow and low-level cyclonic convergence of water vapor, which is more conducive to triggering Extreme precipitation.

Further investigation reveals that the increase in precipitation primarily occurs in the late afternoon and nighttime, and the precipitation distributions exhibit a distinct eastward shift over time. It is found that this eastward shift is exactly consistent with the vertical helicity (Fig. 12 a1–a5) and the westward extension of the WPSH (Fig. 12 b1–b5). This result indicates that the development of low-level cyclones, coupled with the continuous transport of water vapor and the enhancement of the low-level jet stream due to the intensified WPSH associated with steep terrain, contributes to the further increase in precipitation. We also note that the high-value area of the potential vorticity over the EPTP extends from 200 hPa to the surface and is accompanied by strong upward motion over a large topographic gradient (Fig. 11 b1–b5).

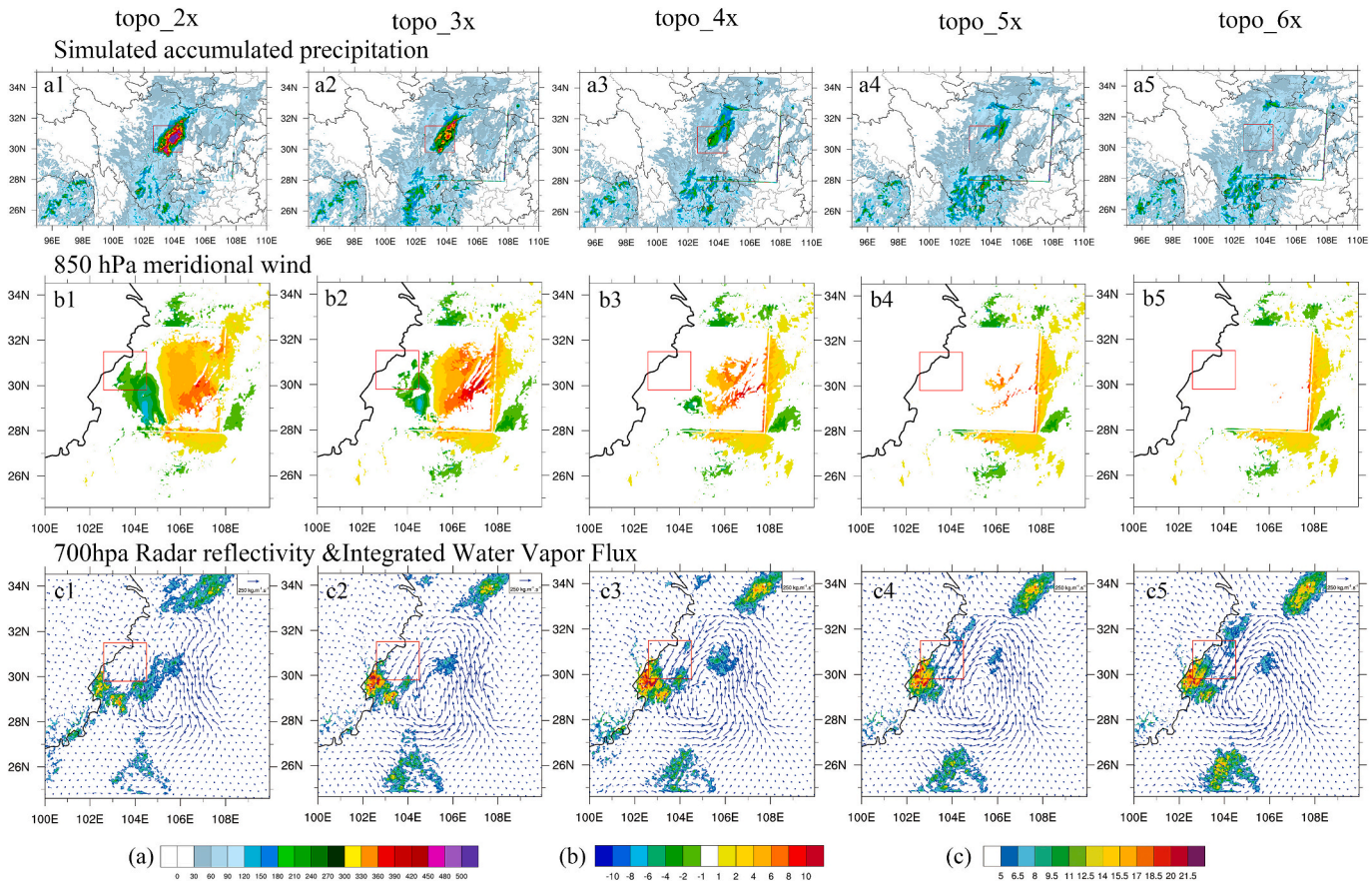

Fig. 10. (a1–a5) Accumulated rainfall on August 15–18, 2020 (mm) simulated with different terrain slopes designed in Fig. 9b, (b1–b5) differences (control experiment minus sensitivity experiment) in 850 hPa meridional wind (color shaded areas), and (c1–c5) radar reflectivity (color shaded areas, dBZ) and integrated water vapor flux (vector, kg m^{-1} s^{-1}).

According to the energy conservation principle of potential vorticity, the vorticity increases when the airflow from the upper-level stable environment reaches the low-level unstable environment. On the one hand, positive vorticity is transferred to the lower levels. On the other hand, the interaction between the dry downdrafts in the upper level and the warm and moist air in the lower troposphere increases potential instability, thus strengthening the occurrence and development of surface cyclones (Hoskins et al., 1985; Shou, 2010). The evolutions of potential vorticity and zonal wind also reveal that positive vorticity is more likely to form in areas with steep terrain, and the meridional transport of westerly wind is more intense (Fig. 12 c1–c5), which suggests that the continuous transport of positive vorticity by westerlies is possibly one of the reasons for the maintenance of Extreme precipitation. This is consistent with the findings of Miao et al. (2019), i.e., the PEP study in South China, which indicates that the meridional wind transport of low-frequency relative vorticity and geostrophic vorticity can intensify and sustain the upward motion over South China for a long time.

4. Conclusions and discussion

4.1. Conclusions

The EPTP is characterized by highly complex topography, with steep slopes exceeding 3000 m. Due to the complex terrain and the combined effects of multiple synoptic systems, the causes of extreme precipitation in this region have not been well investigated. To this end, we first analyzed the characteristics of atmospheric circulation anomalies during the PEP events based on ERA5 reanalysis data and then quantitatively identified the moisture sources responsible for the PEP events in the EPTP based on the constructed Lagrangian moisture source field. Finally, the terrain sensitivity test was implemented to explore the effect of steep terrain on the PEP events. The main conclusions are as follows.

This research found that the configuration of the atmospheric circulation system is characterized by remarkable anomalies during the PEP events in the EPTP. Specifically, the 500 hPa geopotential height exhibited an anomaly structure similar to a Rossby wave train, and the westerly jet stream was enhanced, accompanied by the eastward extension of the SAH and the westward extension of the WPSH. Under the influence of these anomalous atmospheric circulations, the EPTP exhibited pronounced potential instability in the troposphere. The convergent anticyclonic water vapor transport, together with the enhanced southwesterly water vapor, supplied favorable moisture conditions for the PEP. In terms of longer-duration events, the meridional distance between the SAH and the WPSH was closer, accompanied by stronger convergence of warm and cold airflow and a longer duration of low vortex and water vapor convergence.

The PEP events in the EPTP were simultaneously regulated by the East Asian monsoon and the South Asian monsoon. Specifically, the East Asian summer monsoon played a leading role, transporting water vapor to the EPTP through both the East Asia and South China Sea paths. Although the water vapor from NEA is the main moisture contributor in summer (30.84%), the SEA provided the majority of the moisture for the PEP events (38.1%) on a longer time scale (7–10 days). In addition, the water vapor transported by the Indian (South Asian) summer monsoon also played a supporting role (16.38%) on a shorter time scale (4–6 days). In general, the evaporative moisture sources from the SEA, BOB, and SCS are remarkably enhanced during PEP events, with a total contribution of 56.44%, which is 28.5% higher than the climatic mean.

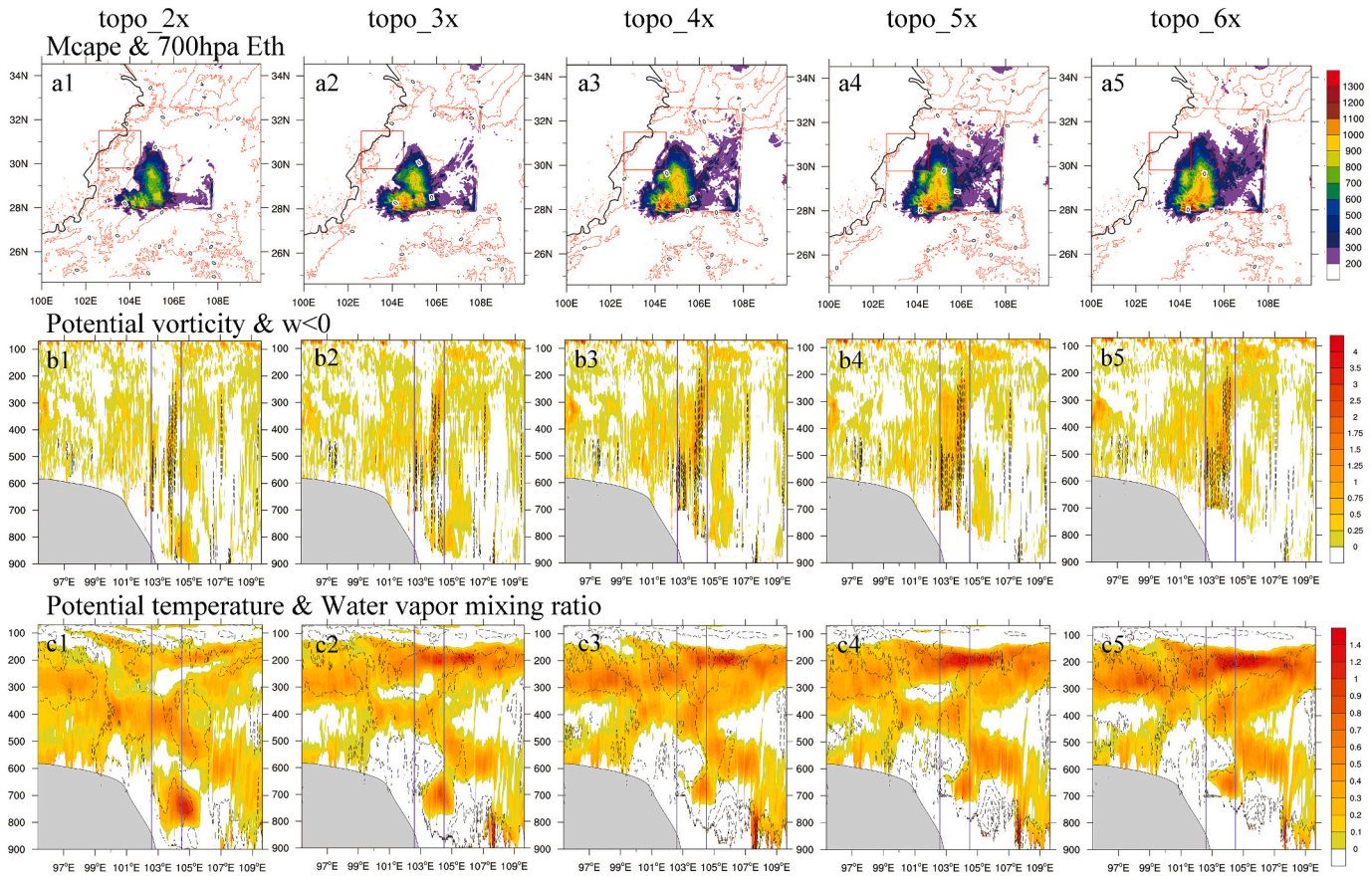

Fig. 11. (a1–a5) Differences (control experiment minus sensitivity experiment) in the maximum convective available potential energy (color shaded areas, J kg^{-1}) and the equivalent potential temperature (solid red lines, K) for different terrain slopes, and vertical profiles of (b1–b5) the potential vorticity (color shaded areas) and (c1–c5) potential temperature (color shaded areas). The black dashed lines in Fig. 11b1–10b5 indicate the areas with vertical velocity below 0, and the black dashed lines in Fig. 11c1–10c5 represent the water vapor mixing ratio. The red rectangle in a1-a5 indicates the EPTP region, so as the solid purple line in b1-b5 and c1-c5.

The terrain sensitivity test revealed that the steep terrain played an important role in the triggering, enhancement and maintenance of the PEP. On the one hand, it places the EPTP in a warm and humid environment with highly unstable energy, where the sufficient convergence of north-south airflow and cyclonic convergence of low-level water vapor was more conducive to the triggering of the Extreme precipitation. On the other hand, the steep terrain resulted in the formation of positive potential vorticity, the continuous transport of positive vorticity and the downward propagation of upper-level isentropic potential vorticity disturbances, further contributing to the intensification and maintenance of precipitation.

4.2. *Discussion*

As a transition zone of the Tibetan Plateau and the Sichuan Basin, the EPTP has attracted a great deal of attention with regarding to its extreme precipitation mechanisms (Chen et al., 2016; Liu et al., 2018; Fu et al., 2019; Mai et al., 2021; Nie and Sun, 2021; Hu et al., 2021; Xu et al., 2023).

Even the topic of this study is particularly concentrated on the PEP events, parts of the results of this study are in agreement with those previous efforts focusing on the general extreme precipitation events. For instance , in terms of large-scale atmospheric circulation configuration, some previous studies have indicated that the PEP events over the TP and its adjacent regions are often accompanied by an anomalous Rossby wave train at middle levels, an intensified westerly jet, together with an eastward extension of the South Asian high and a westward extension of the western Pacific subtropical high (e.g.,Qian et al., 2022; Xu et al., 2023). However, the more factors or physical processes could be involved into the development and maintenance of the circulation anomalies. For instance, it has also been noted that the zonal shifts of WPSH and southern Asian high can be induced by TP heat sources (Ren et al., 2019), and be influenced by the low-latitude Intraseasonal oscillations (Nie and Sun, 2021) and the anomalous disturbances caused by wave trains (Miao et al., 2019).This implies the complexity of the PEP events development, and the mechanisms behind it deserve further exploration.

Regarding to the moisture sources identification, some previous studies have been carried to the single extreme precipitation over the adjacent regions of EPTP (e.g., Huang and Cui, 2015; Chen and Xu, 2016). Comparing to these studies, the study presented herein pointed clearly out that the Southeastern Asia (SEA) act as the dominant terrestrial moisture contributor to the PEP events in EPTP, rather than the Sichuan Basin itself. This result further highlights the essential role of water vapor transport by the large-scale circulation for the occurrence of PEP events. In addition, our results also emphasize the effects of steep topography on the PEP events. Specifically, the continuous transport of positive potential vorticity by zonal wind under the influence of topography is one of the important reasons for the maintenance of PEP events.

Some caveats in the interpretation of these results need to be clarified as well. For instance, this study is mainly based on the “reanalysis” world, the more gauged observations needs to validate the results presented here. Note that the data used in this study is on a daily scale, so it cannot capture the fine structures of PEP events, such as its diurnal evolution (Li, 2018; Zhao et al., 2020). The geohazards and the

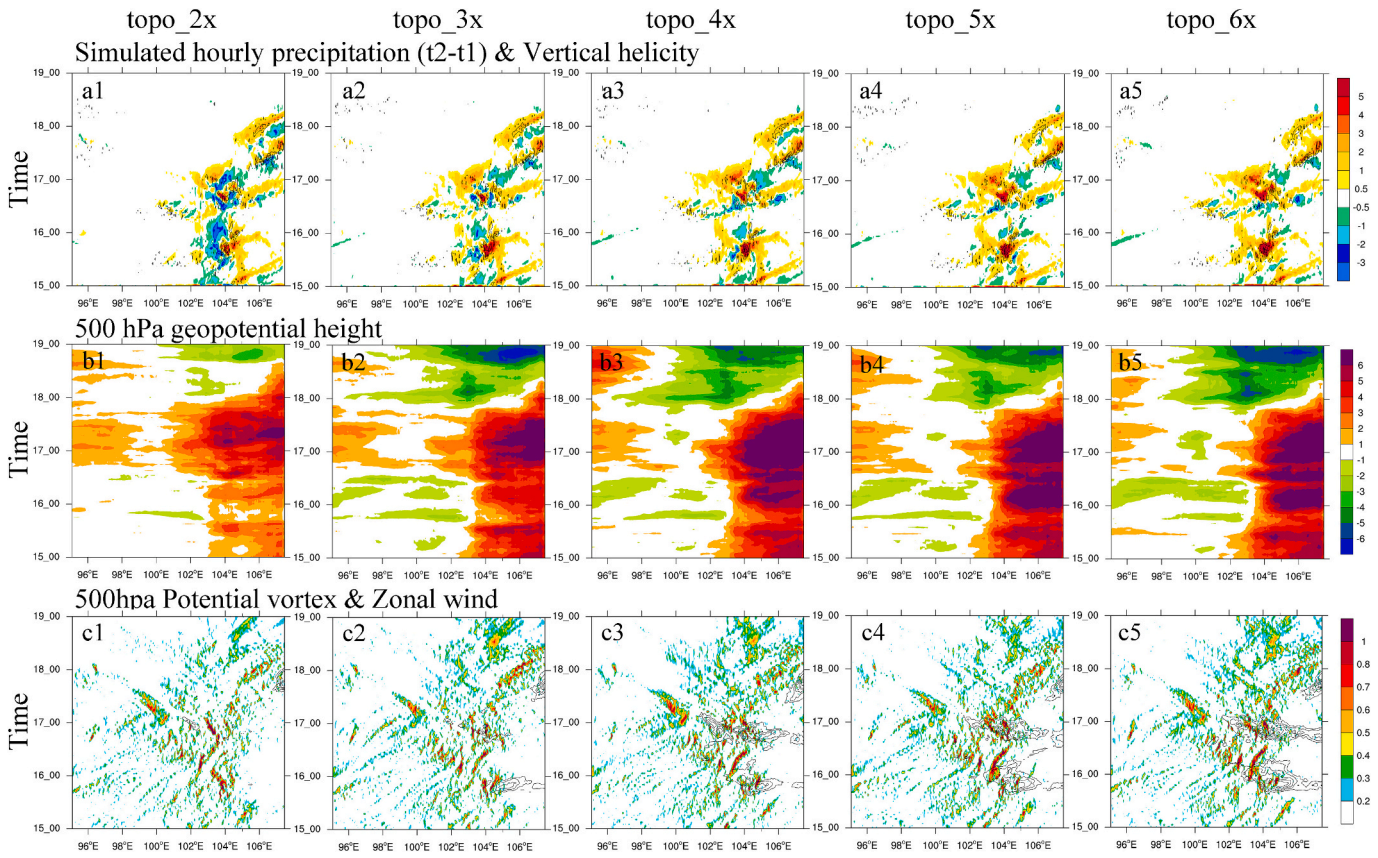

Fig. 12. Time-longitude profiles of the differences (control experiment minus sensitivity experiment and the hour after minus the hour before) in (a1–a5) the simulated hourly precipitation (mm) with different terrain slopes, (b1–b5) 500 hPa geopotential height and (c1–c5) potential vortex (color shaded). The solid black lines in Fig. 12a1–12a5 and 12c1–12c5 indicate the vertical helicity and zonal wind, respectively.

corresponding mechanisms induced by extreme precipitation at hourly scale are different from those at daily scales and more detailed mechanisms are expected in the future research. (Zhao et al., 2020). Additionally, the effects of topography on the precipitation could vary with different scale (Nishizawa et al., 2021), which merit a detailed analysis on different scale.

CRediT authorship contribution statement

Ruiyu Zhao: Visualization, Writing – original draft. **Bin Chen:** Conceptualization, Methodology, Supervision. **Wei Zhang:** Writing – review & editing. **Shuai Yang:** Formal analysis, Investigation, Validation. **Xiangde Xu:** Funding acquisition.

Declaration of competing interest

The authors declare that they have no known competing financial interests or personal relationships that could have appeared to influence the work reported in this paper.

Data availability

Data will be made available on request.

Acknowledgments

This research is supported by The Second Tibeta Plateau Comprehensive Scientific Expedition and Research Program, Grant/Award Number: 2019QZKK0105; the S&T Development Fund of CAMS, Grant/Award Numbers: 2023KJ027, 2021KJ021; The Open Grants of the State Key Laboratory of Severe Weather, Chinese Academy of Meteorological Sciences, Grant/Award Number: 2023LASW-A04; the National Natural Science Foundation of China, Grant/Award Number: 42175010, National Key R&D Program of China, Grant/Award Number: 2023YFC3010700. The observed precipitation compiled by the China Meteorological Administration is available at http://data.cma.cn/. The ERA-Interim dataset can be obtained from http://www.ecmwf1.int. The ERA5 reanalysis could be available from https://cds.climate.copernicus.eu/.

References

Chen, Y.R., Li, Y.Q., 2021. Convective characteristics and formation conditions in an extreme rainstorm on the Eastern Edge of the Tibetan Plateau. Atmosphere 12, 381. https://doi.org/10.3390/atmos12030381.

Chen, B., Xu, X.D., 2016. Spatiotemporal structure of the moisture sources feeding heavy precipitation events over the Sichuan Basin. Int. J. Climatol. 36 (10), 3446–3457.

Chen, D., Zhou, C., Deng, M., 2016. Characteristics of water vapor content in Southwest China and its association with the South Asian high in summer. J. Appl. Meteorol. Sci. 27 (4), 473–479.

Chen, H., Li, J., Yu, R., 2018a. Warm season nocturnal rainfall over the eastern periphery of the Tibetan plateau and its relationship with rainfall events in adjacent regions. Int. J. Climatol. 38, 4786–4801.

Chen, B., Xu, X.-D., Zhao, T., 2018b. Quantifying oceanic moisture exports to mainland China in association with summer precipitation. Clim. Dyn. 51, 4271–4286.

Chen, B., Zhang, W., Yang, S., Xu, X.D., 2019. Identifying and contrasting the sources of the water vapor reaching the subregions of the Tibetan Plateau during the wet season. Clim. Dyn. 53, 6891–6907. https://doi.org/10.1007/s00382-019-04963-2.

Chen, Qian, Yangbo, Ye, Wenxia, Zhang, Tianjun, Zhou, 2022. Heavy rainfall event in Mid-August 2022 in S outhwestern China: contribution of anthropogenic forcings and atmospheric circulation. Bull. Am. Meteorol. Soc. 103 (3), S111–S117.

Dai, Panxi, Nie, Ji, 2022. Robust expansion of extreme midlatitude storms under global warming. Geophys. Res. Lett. 49 https://doi.org/10.1029/2022GL099007.

David, Bolton, 1980. The computation of Equivalent potential Temperature. Mon. Weather Rev. 108 (7), 1046–1053.

Ding, J., Cuo, L., Zhang, Y., Zhang, C., Liang, L., Liu, Z., 2021. Annual and seasonal precipitation and their extremes over the Tibetan Plateau and its surroundings in 1963–2015. Atmos 12, 620.
Dong, W., et al., 2016. Summer rainfall over the southwestern Tibetan Plateau controlled by deep convection over the Indian subcontinent. Nat. Commun. 7, 10925.
Draxler, R.R., Hess, G., 1998. An overview of the HYSPLIT_4 modelling system for trajectories. Aust. Meteor. Mag. 47, 295–308.
Drumond, A., Stojanovic, M., Nieto, R., Vicente-Serrano, S.M., Gimeno, L., 2019. Linking anomalous moisture transport and drought episodes in the IPCC reference regions. Bull. Amer. Meteor. Soc. 100, 1481–1498.
Feng, L., Zhou, T., 2012. Water vapor transport for summer precipitation over the Tibetan Plateau: Multidata set analysis. Journal of Geophysical Research: Atmospheres 117, D20114.
Fu, S.M., Mai, Z., Sun, J.H., Li, W.L., Ding, Y., Wang, Y.Q., 2019. Impacts of convective activity over the Tibetan Plateau on plateau vortex, southwest vortex, and downstream precipitation. J. Atmos. Sci. 76, 3803–3830. https://doi.org/10.1175/JAS-D-18-0331.1.
Gimeno, L., Stohl, A., Trigo, R.M., et al., 2012. Oceanic and terrestrial sources of continental precipitation. Rev. Geophys. 50, RG4003. https://doi.org/10.1029/2012RG000389.
Hersbach, H., Bell, B., Berrisford, P., et al., 2020. The ERA5 global reanalysis. Q. J. R. Meteorol. Soc. 146 (730), 1999–2049.
Hoskins, B.J., McIntyre, M.E., Robertson, A.W., 1985. On the use and significance of isentropic potential vorticity maps. Quart. J. Roy Meteor. Soc. 111, 877–946.
Hu, X.L., Yuan, W.H., 2021. Evaluation of ERA5 precipitation over the eastern periphery of the Tibetan Plateau from the perspective of regional rainfall events. Int. J. Climatol. 41 (4), 2625–2637. https://doi.org/10.1002/joc.6980.
Hu, X.L., Yuan, W.H., Yu, R.C., 2021. The extraordinary rainfall over the Eastern Periphery of the Tibetan Plateau in August 2020. Adv. Atmos. Sci. 38 (12), 2097–2107. https://doi.org/10.1007/s00376-021-1134-7.
Huang, Y.J., Cui, X.P., 2015. Moisture sources of Torrential Rainfall events in the Sichuan Basin of China during Summers of 2009–13. J. Hydrometeorol. 16 (4), 1906–1917.
Jia, Wu, Xuejie, Gao, Filippo, Giorgi, Deliang, Chen, 2017. Changes of effective temperature and cold/hot days in late decades over China based on a high resolution gridded observation dataset. Int. J. Climatol 37 (s1), 788–800. https://doi.org/10.1002/joc.5038.
Kimura, F., Kuwagata, T., 1995. Horizontal heat fluxes over complex terrain computed using a simple mixed-layer model and a numerical model. J. Appl. Meteorol. 34, 549–558. https://doi.org/10.1175/1520-0450-34.2.549.
Koutarou, Takaya, Hisashi, Nakamura, 2001. A formulation of a phase-independent wave-activity flux for stationary and migratory quasigeostrophic eddies on a zonally varying basic flow, 58 (6), 608–627.
Li, J., 2018. Hourly station-based precipitation characteristics over the Tibetan Plateau. Int. J. Climatol. 38 (3), 1560–1570. https://doi.org/10.1002/joc.5281.
Li, Y.Q., Li, D.J., Yang, S., Liu, C., Zhong, A.H., Li, Y., 2010. Characteristics of the precipitation over the eastern edge of the Tibetan Plateau. Meteorog. Atmos. Phys. 106 (1), 49–56.
Li, L., Zhang, R.H., Wu, P.L., Wen, M., Duan, J.P., 2020. Roles of Tibetan Plateau vortices in the heavy rainfall over southwestern China in early July 2018. Atmos. Res. 245, 105059.
Liu, X.L., Ma, E.D., Cao, Z.B., et al., 2018. Numerical study of a southwest vortex rainstorm process influenced by the eastward movement of Tibetan Plateau vortex. Adv. Meteorol. 2018, 9081910.
Liu, R., Wang, X., Wang, Z.L., 2022. Atmospheric moisture sources of drought and wet events during 1979–2019 in the Three-River Source Region, Qinghai-Tibetan Plateau. Theor. Appl. Climatol. 149, 487–499. https://doi.org/10.1007/s00704-022-04058-9.
Lu, N., 2019. Scale effects of topographic ruggedness on precipitation over Qinghai-Tibet Plateau. Atmos Sci Lett 20, e904. https://doi.org/10.1002/asl.904.
Luo, Y.L., et al., 2020. Science and prediction of heavy rainfall over China: research progress since the reform and opening-up of new China. J. Meteorol. Res. 34, 427–459.
Ma, Y., Lu, M., Chen, H., Pan, M., Hong, Y., 2018. Atmospheric moisture transport versus precipitation across the Tibetan Plateau: a mini-review and current challenges. Atmos. Res. 209, 50–58. https://doi.org/10.1016/j.atmosres.2018.03.015.
Ma, Qian R., Fang, J., Xiao, X.W., You, Z.C., Rong, Z., Guo, L.F., 2022. Characteristics and related mechanisms of the persistent extreme precipitation in August 2020 over Western China. Front. Earth Sci. 10, 1004612.
Mai, Z., Fu, S.M., Sun, J.H., et al., 2021. Key statistical characteristics of the mesoscale convective systems generated over the Tibetan Plateau and their relationship to precipitation and Southwest vortices. Int. J. Climatol. 41 (S1), E875–E896.
Meng, Yang, Sun, Jianhua, et al., 2021. A 10-year climatology of mesoscale convective systems and their synoptic circulations in the Southwest Mountain Area of China. J. Hydrometeorol. 22, 23–41. https://doi.org/10.1175/JHM-D-20-0167.1.
Miao, R., Wen, M., Zhang, R.H., et al., 2019. The influence of wave trains in mid-high latitudes on persistent heavy rain during the first rainy season over South China. Clim. Dyn. 53, 2949–2968.
Ni, C.C., Li, G.P., Xiong, X.Z., 2017. Analysis of a vortex precipitation event over Southwest China using AIRS and in situ measurements. Adv. Atmos. Sci. 34 (4), 559–570.
Nie, Y., Sun, J., 2021. Synoptic-scale circulation precursors of extreme precipitation events over Southwest China during the rainy season. J. Geophys. Res. Atmos. 126 https://doi.org/10.1029/2021JD035134.
Nishizawa, S., Yamaura, T., Kajikawa, Y., 2021. Influence of submesoscale topography on daytime precipitation associated with thermally driven local circulations over a mountainous region. J. Atmos. Sci. 78, 2511–2532. https://doi.org/10.1175/JAS-D-20-0332.1.
Pisso, I., Sollum, E., Grythe, H., et al., 2019. The Lagrangian particle dispersion model FLEXPART version 10.4. Geosci. Model Dev. 12, 4955–4997. https://doi.org/10.5194/gmd-12-4955-2019.
Qian, Chen, Zhang, Wenxia, Zhou, Tianjun, 2022. Heavy Rainfall Event in Mid-August 2022 in S outhwestern China: Contribution of Anthropogenic Forcings and Atmospheric Circulation. Bulletin of the American Meteorological Society 103 (3), S111–S117.
Qinglong, You, Shichang, Kang, Enric, Aguilar, et al., 2008. Changes in daily climate extremes in the eastern and central Tibetan Plateau during 1961—2005. J. Geophys. Res.-Atmos. 113 (D7), 1639–1647. https://doi.org/10.1029/2007jd009389.
Ren, X., Yang, D., Yang, X., 2015. Characteristics and Mechanisms of the Subseasonal Eastward Extension of the South Asian High. J. Climate 28, 6799–6822. https://doi.org/10.1175/JCLI-D-14-00682.1.
Ren, R., Zhu, C., Cai, M., 2019. Linking quasi-biweekly variability of the South Asian high to atmospheric heating over Tibetan Plateau in summer. Clim. Dyn. 53, 3419–3429. https://doi.org/10.1007/s00382-019-04713-4.
Samel, A.N., 2003. Understanding Relationships between the 1998 Yangtze River Flood and Northeast Eurasian Blocking. Climate Research 23, 149–158. https://doi.org/10.3354/cr023149.
Shenming, Fu, Wanli, Li, Jianhua, Sun, et al., 2015. Universal evolution mechanisms and energy conversion characteristics of long-lived mesoscale vortices over the Sichuan Basin. Atmos. Sci. Lett. 16, 127–134. https://doi.org/10.1002/asl2.533.
Shi, X., Wang, Y., Xu, X., 2008. Effect of mesoscale topography over the Tibetan Plateau on summer precipitation in China: a regional model study. Geophys. Res. Lett. 35, L19707. https://doi.org/10.1029/2008GL034740.
Shou, S.W., 2010. Theory and application of potential vorticity, 36 (03), 9–18 (in chinese).
Smith, R.B., 1989. Hydrostatic airflow over mountains. Adv. Geophys. 31, 1–41. https://doi.org/10.1016/S0065-2687(08)60052-7. Elsevier.
Sodemann, H., Schwierz, C., Wernli, H., 2008. Interannual variability of Greenland winter precipitation sources: Lagrangian moisture diagnostic and North Atlantic Oscillation influence. J. Geophys. Res. 113, D03107. https://doi.org/10.1029/2007JD008503.
Sokol, Z., Bližňák, V., 2009. Areal distribution and precipitation–altitude relationship of heavy short-term precipitation in the Czech Republic in the warm part of the year. Atmos. Res. 94 (4), 652–662.
Sprenger, M., Wernli, H., 2015. The LAGRANTO Lagrangian analysis tool - version 2.0. Geosci. Model Dev. 8 (8), 2569–2586. https://doi.org/10.5194/gmd-8-2569-2015.
Stohl, A., James, P., 2004. A Lagrangian analysis of the atmospheric branch of the global water cycle. Part I: method description, validation, and demonstration for the August 2002 flooding in Central Europe. J. Hydrometeorol. 5, 656–678. https://doi.org/10.1175/1525-7541(2004)005,0656: ALAOTA.2.0.CO;2.
Stohl, A.P. James, et al., 2005. A Lagrangian analysis of the atmospheric branch of the global water cycle. Part II: moisture transports between Earth's ocean basins and river catchments. J. Hydrometeorol. 6, 961–984. https://doi.org/10.1175/JHM470.1.
Sun, B., Wang, H., 2014. Moisture sources of semi-arid grassland in China using the Lagrangian Particle Model FLEXPART. J. Clim. 27, 2457–2474. https://doi.org/10.1175/JCLI-D-13-00517.1.
Trenberth, K.E., 1998. Atmospheric moisture residence times and cycling: implications for rainfall rates and climate change. Climate Change 39 (4), 667–694.
Trenberth, K.E., 1999. Atmospheric moisture recycling: role of advection and local evaporation[J]. J. Clim. 12, 1368–1381. https://doi.org/10.1175/1520-0442(1999)0122.0.CO;2.
Tuel, A., Martius, O., 2022. Subseasonal temporal clustering of extreme precipitation in the northern hemisphere: regionalization and physical drivers. J. Clim. 35 (11), 3537–3555. https://doi.org/10.1175/jcli-d-21-0562.1.
Pan, C., Zhu, B., Gao, J., et al., 2018. Quantitative identification of moisture sources over the Tibetan Plateau and the relationship between thermal forcing and moisture transport [J]. Climate Dynamics. https://doi.org/10.1007/s00382-018-4130-6.
Wang, B., Ho, L., 2002. Rainy season of the Asian-Pacific summer monsoon. J. Clim. 15 (4), 386–398. https://doi.org/10.1175/1520-0442(2002)0152.0.CO;2.
Wang, C.H., Zhou, S.W., Tang, X.P., et al., 2011. Temporal and spatial distribution of heavy precipitation over Tibetan Plateau in recent 48 years. Sci. Geogr. Sin. 31 (04), 470–477 (in chinese). 10.13249/j.cnki.sgs.2011.04.017.
Wang, B., Isidoro, Orlanski, 1987. Study of a Heavy Rain Vortex Formed over the Eastern Flank of the Tibetan Plateau. Monthly Weather Review 115 (7), 1370–1393. https://doi.org/10.1175/1520-0493(1987)115<1370:SOAHRV>2.0.CO;2.
Wu, J., Gao, X.J., 2013. A gridded daily observation dataset over China region and comparison with the other datasets. Chin. J. Geophys. 56 (4), 1102–1111 doi: 10.6038g20130406 (in Chinese).
Wu, M.G., Luo, Y.L., 2019. Extreme hourly precipitation over China: research progress from 2010 to 2019. Torrent. Rain Disast. 38 (5), 502–514. http://www.byzh.org.cn/CN/abstract/abstract2606.shtml.
Xia, R.D., Luo, Y.L., Zhang, D.-L., Li, M.X., Bao, X.H., Sun, J.S., 2021. On the diurnal cycle of heavy rainfall over the Sichuan Basin during 10–18 August 2020. Adv. Atmos. Sci. 38 (12), 2183–2200.
Xu, X., Zhao, T., Lu, C., Guo, Y., Chen, B., Liu, R., Li, Y., Shi, X., 2014. An important mechanism sustaining the atmospheric "water tower" over the Tibetan Plateau. Atmos. Chem. Phys. 14 (20), 11287–11295.
Xu, X., Huang, A., Huang, D., Zhang, Y., Gu, C., Cai, S., et al., 2023. What are the dominant synoptic patterns leading to the summer regional hourly extreme precipitation events over central-eastern Tibetan Plateau and Sichuan Basin? Geophys. Res. Lett. 50, e2022GL102342 https://doi.org/10.1029/2022GL102342.

Yang, J., Wang, B., Wang, B., Bao, Q., 2010. Biweekly and 21–30-day variations of the subtropical summer monsoon rainfall over the lower reach of the Yangtze River Basin. J. Clim. 23, 1146–1159.

Yang, K., Chen, J., Lu, C., Li, J., Liu, T., Deng, L., Li, Y., 2022. Impacts of regional uplift of the Tibetan Plateau on local summer precipitation and downstream moisture budget: a simulation study. Int. J. Climatol. 1–22 https://doi.org/10.1002/joc.7781.

Yi, Zhou, Guo Yunyun, Yu, Fang., 2020. Analysis of a rainstorm process under the joint action of westerly trough and Typhoon in Sichuan Basin. Plateau Mount. Meteorol. Res. 40 (2), 11–17. https://doi.org/10.3969/j.issn.1674-21842020.02.002.

Yuan, J.P., Zhao, D., Yang, R.W., Yang, H.F., 2018. Predecessor rain events over China's low-latitude highlands associated with Bay of Bengal tropical cyclones. Clim. Dyn. 50 (3–4), 825–843.

Yunfei, Fu, et al., 2020. Land surface processes and summer cloud-precipitation characteristics in the Tibetan Plateau and their effects on downstream weather: a review and perspective. Natl. Sci. Rev. https://doi.org/10.1093/nsr/nwz226.

Zhang, C., Tang, Q., Chen, D., 2017a. Recent changes in the moisture source of precipitation over the Tibetan Plateau. J. Clim. 30 (5), 1807–1819.

Zhang, Q., Zheng, Y., Singh, V.P., Luo, M., Xie, Z., 2017b. Summer extreme precipitation in eastern China: mechanisms and impacts. J. Geophys. Res. Atmos. 122, 2766–2778.

Zhang, C., Tang, Q., Chen, D., van der Ent, R.J., Liu, X., Li, W., Haile, G.G., 2019. Moisture source changes contributed to different precipitation changes over the Northern and Southern Tibetan Plateau. J. Hydrometeorol. 20 (2), 217–229.

Zhao, Y., Huang, A., Kan, M., Dong, X., Yu, X., Wu, Y., et al., 2020. Characteristics of hourly extreme precipitation along the Yangtze River Basin, China during warm season. Sci. Rep. 10 (1), 1–13. https://doi.org/10.1038/s41598-020-62535-5.

Zhou, B., Wang, Z., 2019. Enlightenment from heavy autumn rain of West China in 2017: synergic role of atmospheric circulation at mid-high latitudes and oceanic background. Theor. Appl. Climatol. 138, 263–274.

Zhou, Y.S., Yan, L., Wu, T.Y., et al., 2019. Comparative analysis of two rainstorm processes in Sichuan Province affected by the Tibetan Plateau vortex and Southwest vortex. Chin. J. Atmos. Sci. 43 (04), 813–830 (in chinese).